HIGH-TEMPERATURE DIFFUSION OF POTASSIUM IN SILICA

BY

BENJAMIN SCHROCK

A THESIS
SUBMITTED TO THE FACULTY OF

ALFRED UNIVERSITY

IN PARTIAL FULFILLMENT OF THE REQUIREMENTS
FOR THE DEGREE OF

MASTER OF SCIENCE

IN

GLASS SCIENCE

ALFRED, NEW YORK

APRIL, 2022

HIGH-TEMPERATURE DIFFUSION OF POTASSIUM IN SILICA

BY

BENJAMIN SCHROCK

B.S. BUCKNELL UNIVERSITY (2013)

SIGNATURE OF AUTHOR_____

APPROVED BY_____

Dr. WILLIAM LACOURSE, ADVISOR

_____

Dr. ALEXIS CLARE, ADVISORY COMMITTEE

_____

Dr. DORIS MÖNCKE, ADVISORY COMMITTEE

_____

Dr. YIQUAN WU, CHAIR, ORAL THESIS DEFENSE

ACCEPTED BY_____

GABRIELLE GAUSTAD, DEAN
KAZUO INAMORI SCHOOL OF ENGINEERING

ACKNOWLEDGMENTS

I would not have been able to complete this thesis without the support of several people.

First and foremost, I am thankful every day for my beautiful wife Shilah. She made this work possible by caring for our two small boys during countless nights and weekends to give me time to work. In addition, she is my main editor. The words you are about to read have been thoroughly edited by Shilah, including this paragraph.

I would like to thank my thesis advisor Dr. William LaCourse, who carved time out of his demanding teaching schedule to mentor me through this process. I learned a great deal from him and am grateful for all his guidance, constructive criticism, positivity, and flexibility over the past couple of years.

I would also like to acknowledge my colleagues: Samuel Stewart and Craig Nie for our discussions on concentration calculations and derivation, and Sushmit Goyal for his assistance with the Anderson-Stuart model.

TABLE OF CONTENTS

LIST OF TABLES

Page

LIST OF FIGURES

Page

ABSTRACT

This work focuses on determining the diffusion coefficient of potassium in silica at high temperatures. Understanding this diffusion helps predict the final profile of optical fiber. This work also investigates several variables that may affect the potassium diffusion rate: viscous flow, oxygen diffusion, and water diffusion. The glass used in this experiment was HSQ300, a silica glass from Heraeus. The core of the glass cane was doped with ~1.2mol% potassium oxide. The cane underwent thermal cycling, then gradient index measurements were taken to trace the movement of potassium. Four thermal cycles were made on a glass-working lathe with a traversing set of hydrogen-oxygen burners that heated the cane for 31.5 minutes per cycle. The cane's surface was heated to 2256°C, and the equivalent temperature for diffusion in the core was calculated to be 1865°C. After four thermal cycles, the gradient index data showed a diffusion distance of 1.70mm. This resulted in a diffusion coefficient for potassium in silica $D = (1.23 \pm 0.54) \times 10^{-6}$ cm^2/second. Further analysis indicated that potassium diffusion rate may have been influenced by water which diffused into the glass from the hydrogen-oxygen burner.

I. INTRODUCTION

Optical fibers are the pipelines used to send data in the form of light signals around the world at every moment of every day. Nearly everyone uses such fibers, but few know how the abundant properties of glass can be harnessed to better transmit light through the fiber.

To turn a glass preform into an optical fiber, the tip of the preform is heated to over 2000°C and then pulled into a thin strand measuring just 125μm in diameter. The preform is made of at least two different types of glass: the core and the cladding. Each glass has a different refractive index, and light remains in the core due to total internal reflection. The change in chemistry from core to cladding can be characterized by measuring the radial refractive index gradient (profile) across the preform. The "core-clad" structure of such a (failed) preform is shown in Figure 1.

The index profile is formed during fabrication of the preform by controlled diffusion of dopants into the core region. The most commonly used dopant is potassium since it has been shown to decrease viscosity, reduce Rayleigh scattering losses in the fiber [1][16], and be more effective than sodium in altering the refractive index. The potassium composition profile determines the index gradient, and the compositional gradient is determined by potassium mass transport rates at the extent processing conditions, which involve temperatures around 2000°C.

It is difficult to study glass at such high temperatures because it is difficult to maintain high temperatures for the time required for diffusion. The glass is harder to control, more variables can be introduced, and there is less research on the topic from which one can learn. Some studies of pure potassium diffusion in glass exist, but only a small fraction studied low concentrations of potassium at high temperatures. Table I lists the supporting literature found in preparation for this study: published diffusion coefficients for potassium in vitreous silica.

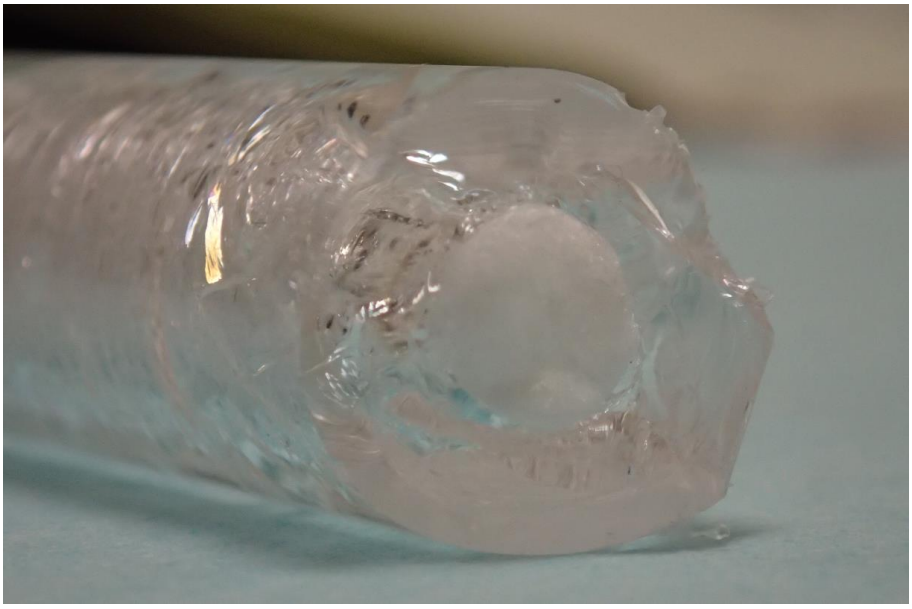

Figure 1: The cross-section of a devitrified cane shows a highly crystallized core with a fractured cladding. The core contracted and separated from the pure silica cladding upon cooling.

Table I: Diffusion Coefficients for Low Potassium Concentrations in Silica Glass at Various Temperatures [1],[2],[3],[4].

Source	D for K^+ [cm^2/s]	Temp for Diffusion [°C]
Frischat, G.	3.5×10^{-12}	300-500
Rothman et al.	1.5×10^{-8}	1000
Smith, C.	$(5\text{-}8) \times 10^{-8}$	1000
Tamura, Y. et al.	4×10^{-6}	2000-2300

In Table I the coefficient found by Frischat [3] was an experiment carried out at "low" temperatures. Even though Smith [4] and Rothman [2] used similar temperatures, and their diffusion coefficients are in relatively good agreement. There are subtle difference between them which may very well be experimental error or it may indicate that other factors affected their diffusion rates.

The Sumitomo patent published by Tamura [1] seems to be the only work that used high temperatures employed in preform fabrication. They did not state their potassium concentration, but they wrote that the concentration in the glass fiber was between 0.2ppm – 100ppm, so their preforms should have had less than 5mol%. Furthermore, their glass contained fluorine, which could have affected their diffusion rate.

II. METHODS AND RESULTS

Because of the challenges of working at 2000°C and higher, initial experiments were carried out with glasses treated at low temperatures for longer periods of time. In one of those early experiments a glass cane was placed in a furnace at 750°C for four weeks. At the end of each week, the cane was removed and cooled, the gradient index was measured, and the cane was returned to the furnace. After 655 hours, the diffusion of potassium was too subtle to significantly change the cane's profile.

Additional experiments were done at temperatures up to 1050°C, but the potassium still did not show any significant mobility. At those temperatures, the potassium-doped core would devitrify, preventing profile measurements. Figure 1 shows a devitrified cane. Upon cooling, the core changed to potassium silicate and cristobalite and separated from the cladding, which fractured due to thermal stress.

At this point, despite the experimental difficulties, it was decided to use a high temperature process similar to that employed in actual production.

A. Method Summary

Potassium was deposited into the core of glass tubes using inside vapor deposition. These tubes were collapsed into canes on a horizontal glass-working lathe equipped with a hydrogen-oxygen burner.

Thermal cycling was performed on the same horizontal lathe. Each heating cycle was a single pass of the burner, and each preform underwent four cycles. A pyrometer and a thermal camera collected data during the heating cycle. After each thermal cycle a preform analyzer measured the gradient index across the preform. This index data was then analyzed to track the movement of potassium in the preform.

B. Glass Preforms

The glass samples used in this experiment were pure silica canes of Heraeus HSQ300. The canes varied in length, but they all had a diameter of about 15mm. The canes' cores were doped with about 2wt% of potassium. The canes had pure silica endcaps to contain the potassium. An alkali salt such as potassium iodide (KI) or potassium bromide (KBr) was vaporized and mixed with pure oxygen through the inside vapor deposition (IVD) process to dope the cores with K_2O. Then the viscous tube was collapsed on a horizontal glass-working lathe, as explained by Lewis [5], Klupsch and Pan [6], and Kirchhof [7]-[12]. This is a common method used in preform fabrication.

C. Gradient Index Measurement

The P106 Preform Analyzer made by Photon Kinetics [13] was used to provide a nondestructive measurement to characterize the potassium in the core. To reduce potential sources of error, the same preform analyzer was used for these measurements. Figure 2 shows the P106 taking a measurement.

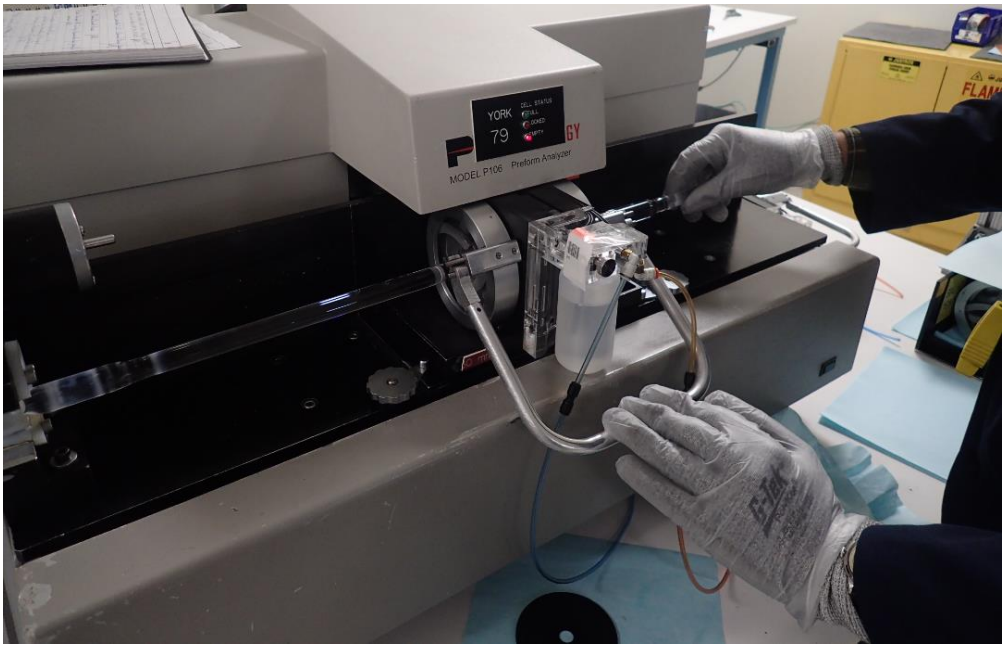

Figure 2: The P106 Preform Analyzer was used to measure the gradient index of the cane.

This preform analyzer does not directly; measure refractive index rather, the index is derived from measuring beam deflection angles. The preform analyzer steps a laser radially across the cane, measures the angle of incidence, and then derives the index properties of the material, as described by Watkins [14].

The preform analyzer provides data in the format of x, n_Δ where x is the distance radially across the cane, and n_Δ is the refractive index difference from the pure silica cell inside the machine. The refractive index difference is defined in Equation 1.

Equation 1
$$n_\Delta = n(\lambda) - n(\lambda)_{SiO_2}$$

Figure 3 shows the raw gradient index data, with labeled points of interest. Before it reaches the cane, the laser passes through the pure silica cell inside the machine. Therefore, the edges of the plot are $0n_\Delta$. Then the laser passes through an oil which surrounds the cane and has a lower gradient index than silica. The steep increase at -7mm and decrease at +7mm mark the surface of the cane and show the difference between pure silica and the HSQ300 glass cane. Trace elements in HSQ300 give it a higher index gradient than pure silica. Table II shows data from Heraeus detailing the chemical purity of their HSQ300 glass [15]. When the laser enters the center of the cane, the gradient index increases because the core is doped with potassium. In this work, a measurement like the one in Figure 3 which technically can be call a gradient index delta from pure silica, is referred to as the gradient index to be concise.

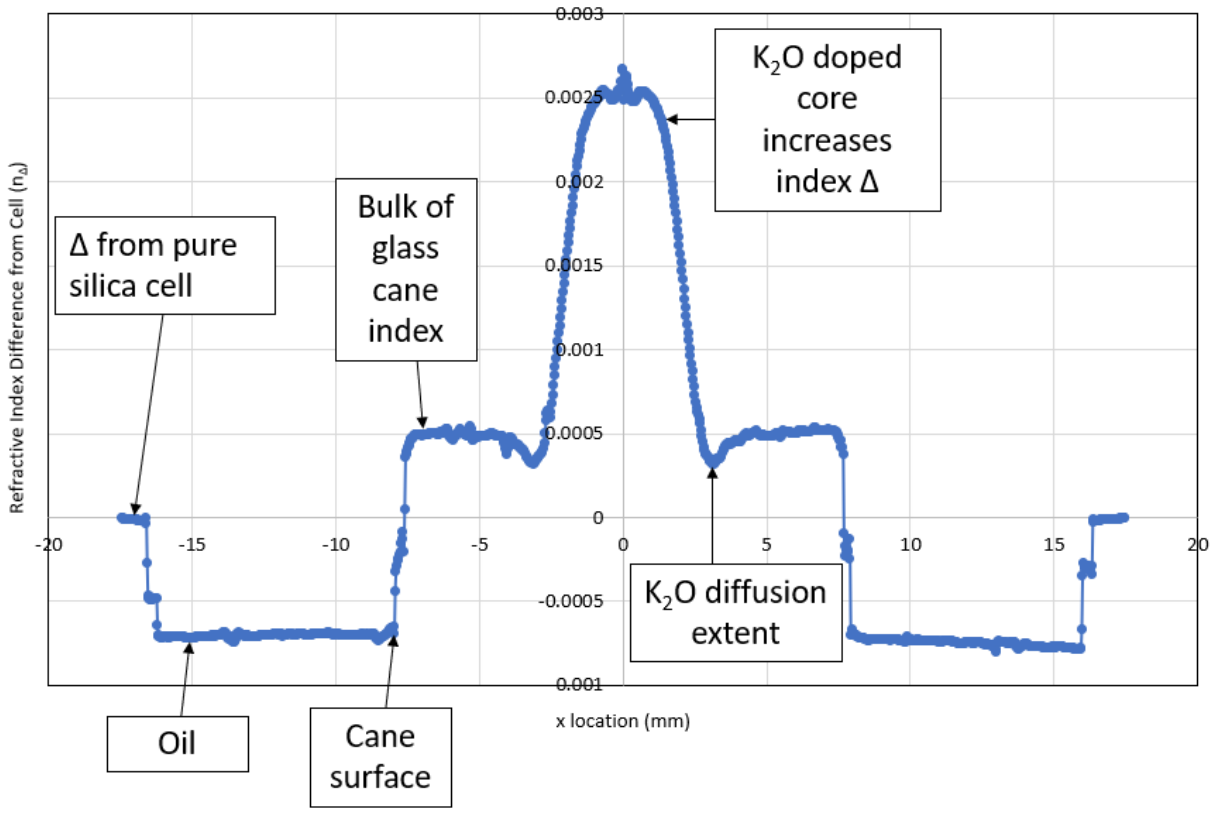

Figure 3: The raw gradient index data from the preform analyzer shows the characteristics of the cane.

Table II: Chemical Purity Data from Heraeus Listing Trace Elements (in PPM) in their HSQ300 Glass.

Li	Na	K	Mg	Ca	Fe	Cu	Cr	Ni	Mn	Ti	Zr	Al	OH
0.5	0.2	0.3	<0.03	0.5	0.1	<0.01	<0.01	<0.01	<0.03	1.1	1	15	<30

D. Thermal Cycle Equipment

For thermal cycling, the canes were placed in a horizontal glass-working lathe (Litton EE255) and rotated while a six-flame, hydrogen-oxygen burner traversed the length of the cane. The slowly rotating spindle prevented the glass from slumping, like a gaffer rotating a blowpipe. The peak surface temperature of the glass above the burner was maintained at 2180°C as measured by a LumaSense Technologies pyrometer (IN 5/5 plus Laser MB 25, a=300, 5.14μm). The pyrometer was focused on the hot zone and used to collect surface temperature data. It was calibrated from 400°C to 2500°C and had a spot size of 6mm. Figure 4 shows a cane being thermally cycled with the pyrometer above.

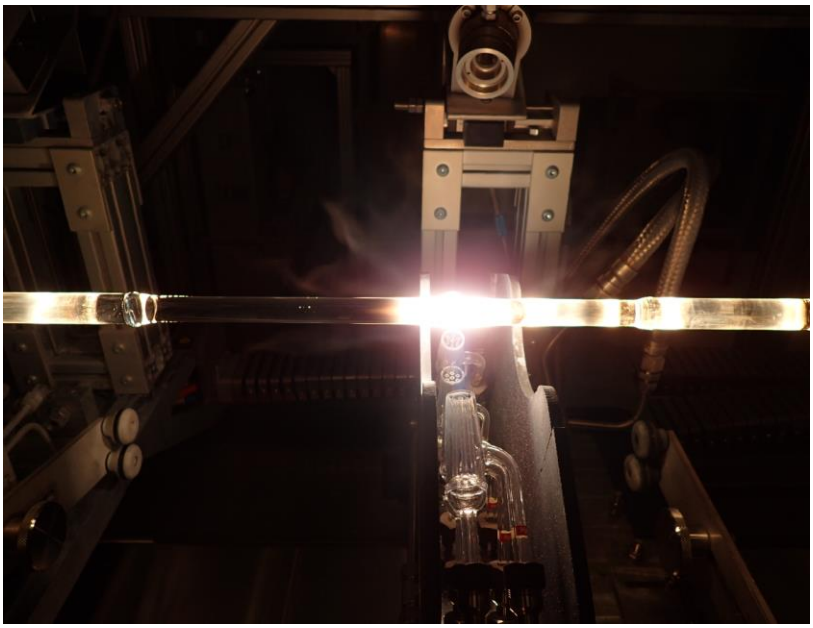

Figure 4: A glass cane in the horizontal lathe, with the hydrogen-oxygen burner below and a pyrometer above the cane.

To control the time of each thermal cycle, the burner was mounted on a flame carriage with a servo motor set to a constant speed of 2mm/min. The traversing burner uniformly heated the cane, except for the very ends where the burner turned off, and the cane quickly cooled. Figure 5 and Figure 6 show the pyrometer data for the cane charted over length and time, respectively.

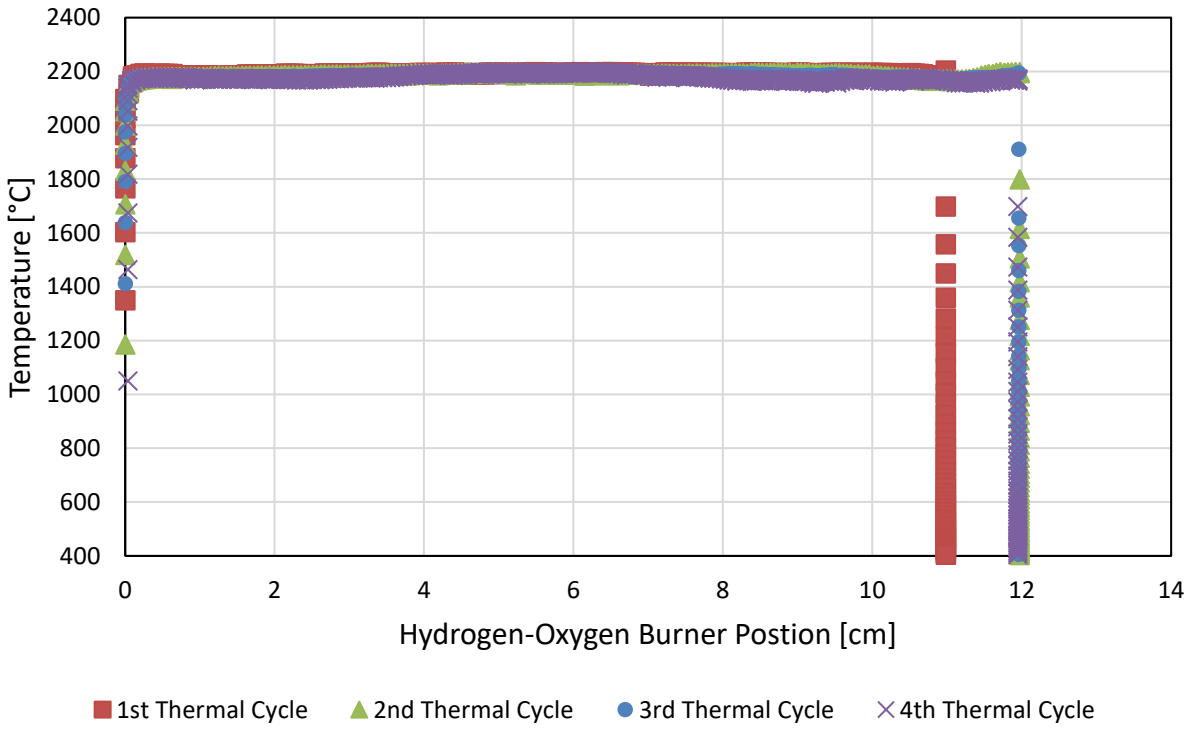

Figure 5: The pyrometer data of three thermal cycles of a glass cane as the burner traversed down the length of the cane at a rate of 2mm/min.

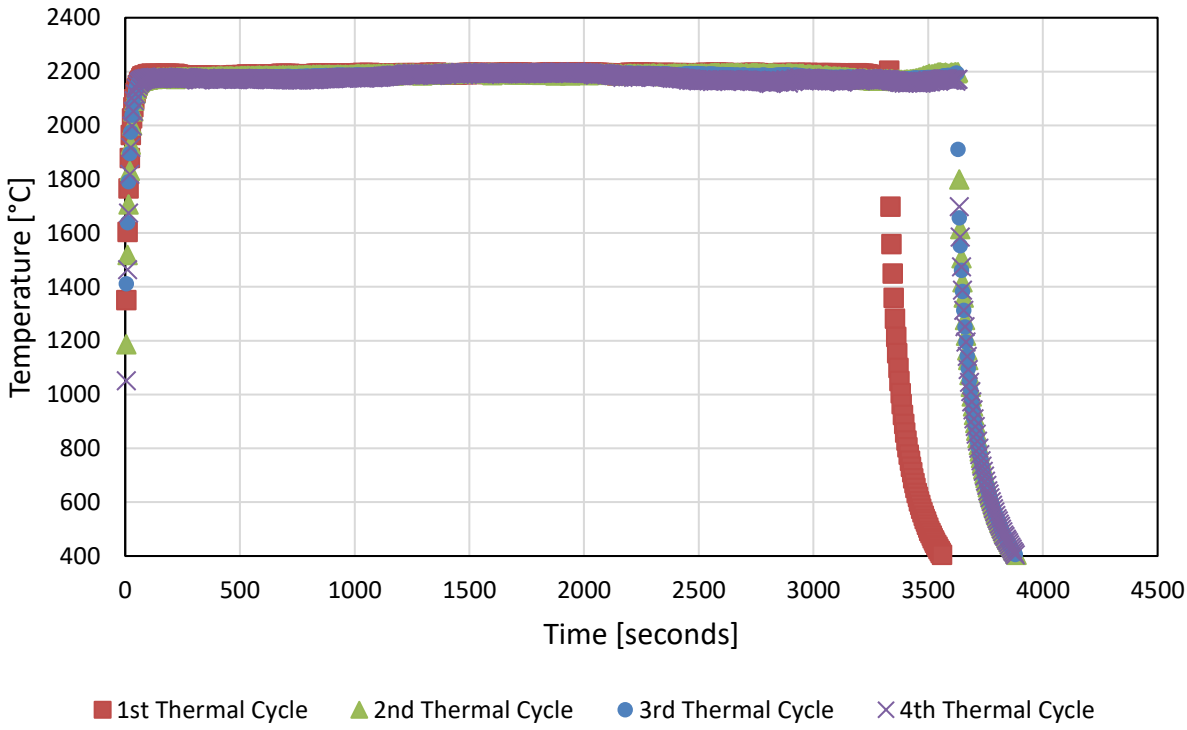

Figure 6: The pyrometer data over time for an 11cm-long glass cane with the hydrogen-oxygen burner traversing at a rate of 2mm/min

Figure 7 shows the end of the cane shortly after the burner turned off. The potassium-doped core on the left radiates brighter as the cane cools. The pure silica end cap glass on the right has no potassium core.

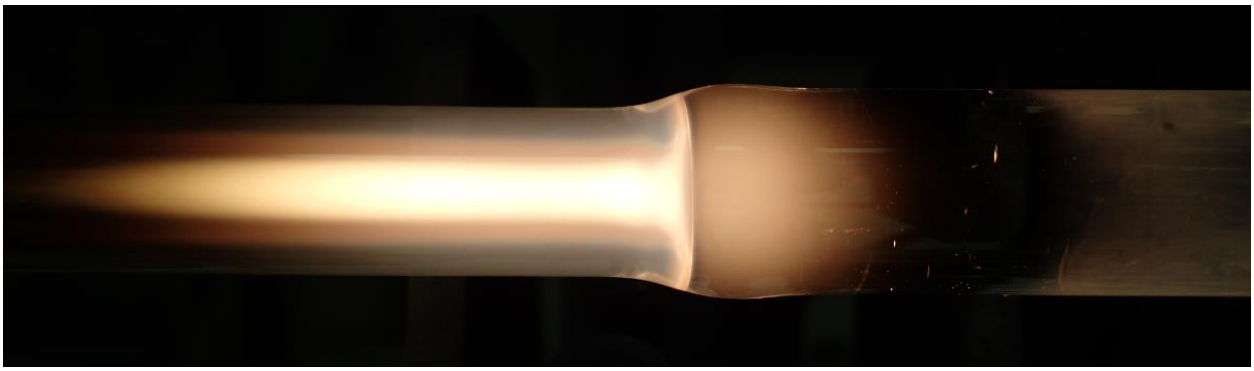

Figure 7: At the end of the thermal cycle the burner shut off, the cane cooled, and the radiating potassium core became visible. The pure silica glass on the right has no potassium core.

The pyrometer data in Figure 8 captures the cooling rate at the end of the run. In about five minutes, the cane cooled to temperatures below the detection limit of the pyrometer. To avoid potential thermal stresses from the rapid cooling zone, the gradient index data was collected at the midpoint of the cane.

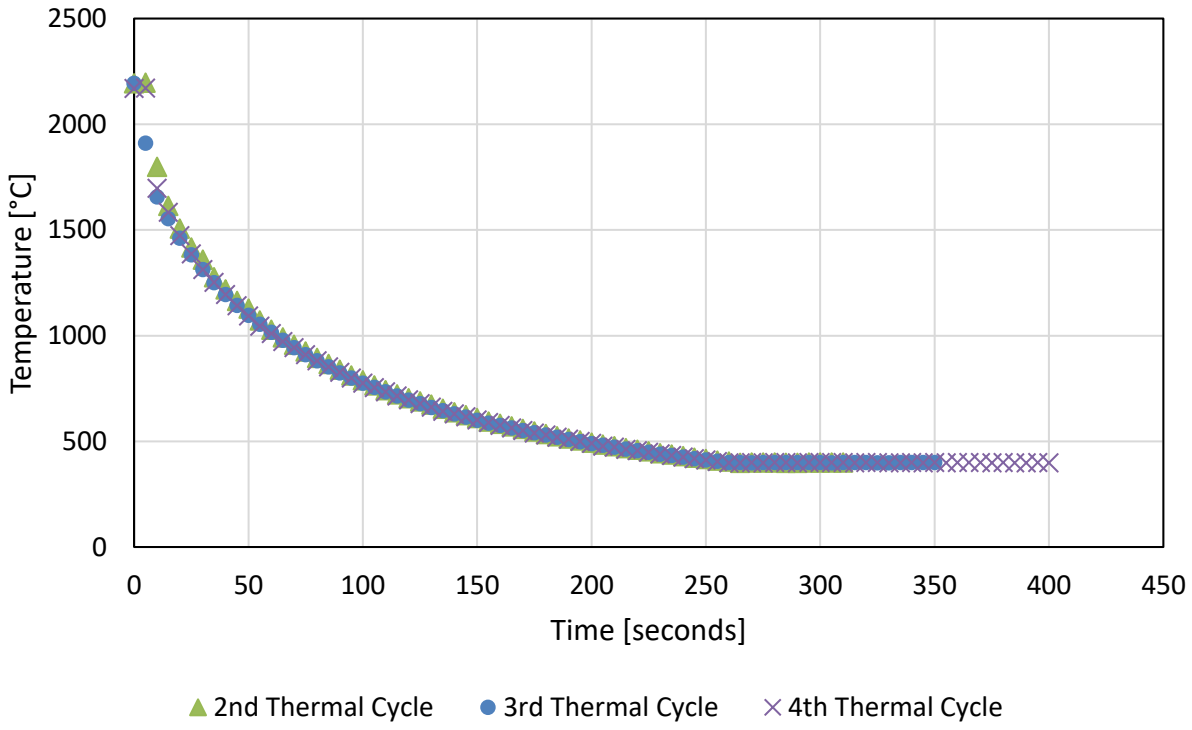

Figure 8: The cooling curve at the end of the run when the burner shut off. In about five minutes, the cane cooled to temperatures below the detection limit of the pyrometer.

E. Thermal Profile

An infrared camera and its corresponding software (FLIR Thermovision A40 and ThermaCAM Researcher Professional 2.0) were used to capture the thermal profile. This camera has a lower limit of 300°C and an upper limit of 2000°C, but the software can be used to linearly extrapolate above 2000°C. For this experiment, the camera's temperature range was set to a minimum of 100°C and a maximum of 2200°C. While this range may cause slight inaccuracies in readings above 2000°C, it can provide good thermal trends and profile shape.

Figure 9 is an image captured by the infrared camera showing the thermal profile of the hot zone. Figure 10 shows the surface temperature of the cane as measured by the camera. The curve flattens as the temperature reaches the 2200°C limit.

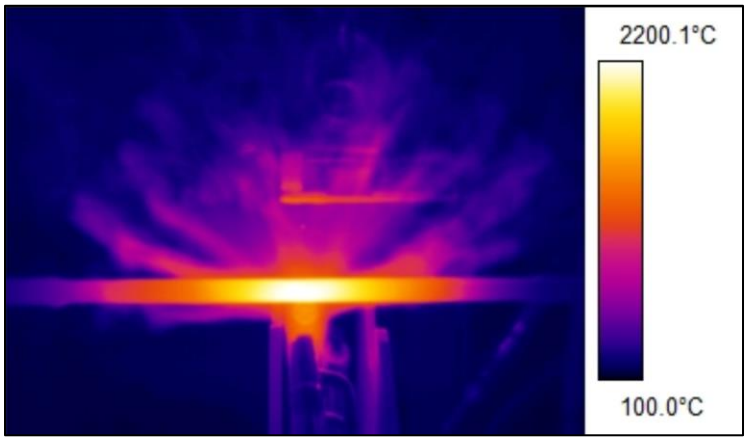

Figure 9: An image from the infrared camera showing the cane in the hot zone.

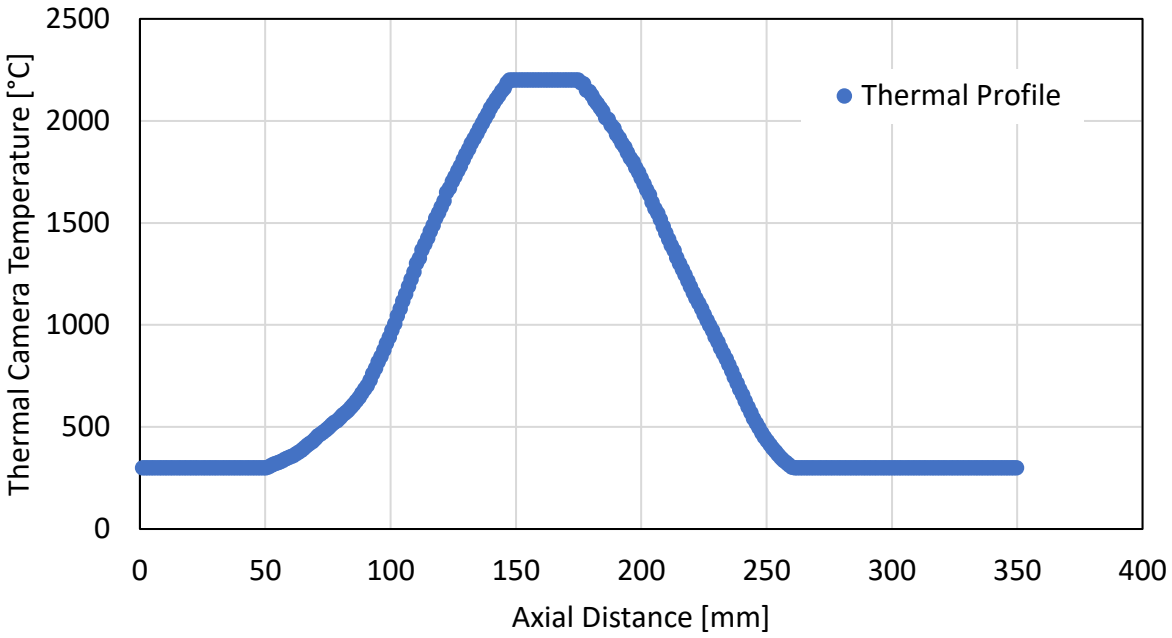

Figure 10: Data from the infrared camera shows the thermal profile. The profile flattens as the 2200°C limit is reached.

Thermal profile data and burner speed can be used to determine heating and cooling rates. Figure 11 shows the heating and cooling curves.

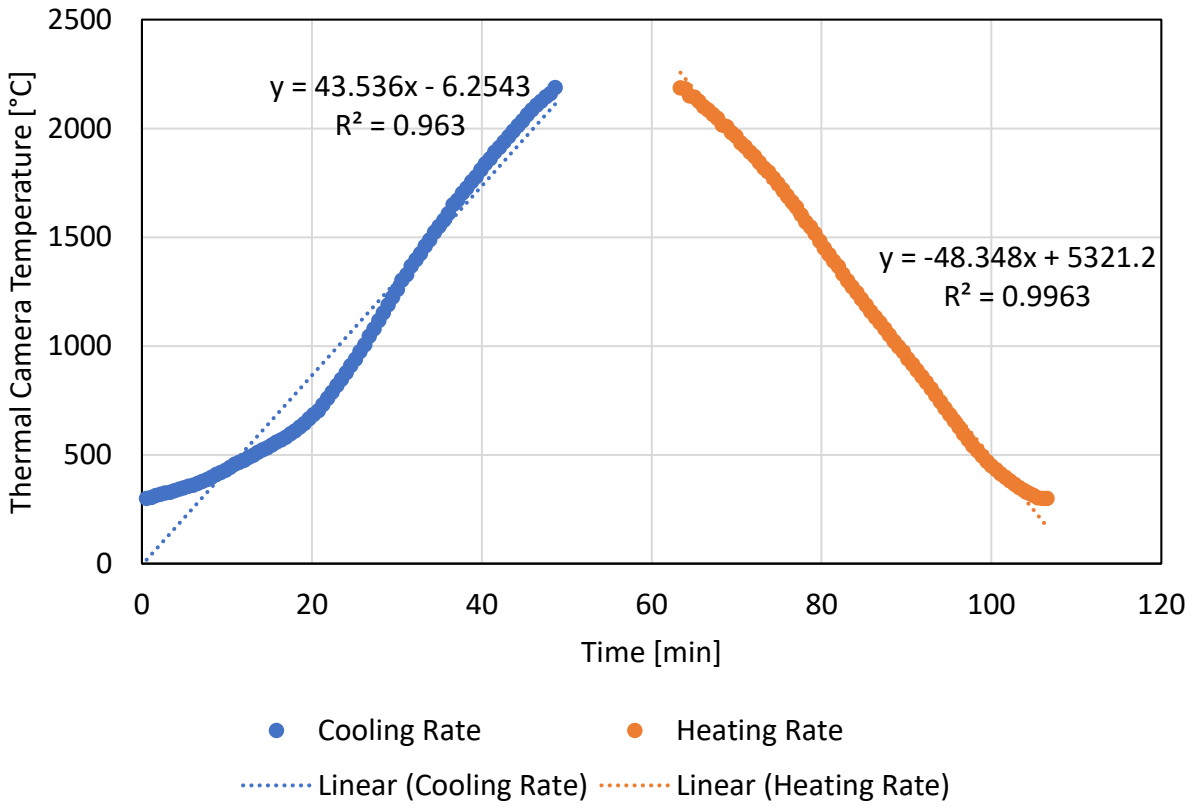

Figure 11: Heating and cooling curves from infrared camera data. The burner traveled from left to right, so the heating curve is on the right, and the cooling rate is on the left.

The burner traveled from left to right, so the heating curve is on the right with a 48°C/min increase, and the cooling rate is on the left with a 44°C/min decrease. The cooling rate is slower because the inside of the cane continues to heat the surface as the cane cools.

This data can be used to determine the total time at an equivalent temperature, which will be needed to calculate the diffusion coefficient.

F. Gradient Index Profiles

After each thermal cycle, the gradient index was measured using the P106 preform analyzer. The measurement was taken at the mid-point along the length of the cane because that location was the most evenly heated and cooled. Then the cane was rotated about its axis by 90°, and the measurement was repeated. The two measurements were averaged to ensure accuracy.

Figure 12 shows two gradient index measurements with the average overlayed. Figure 13 shows the gradient index profiles (averages of the two measurements) for each thermal cycle.

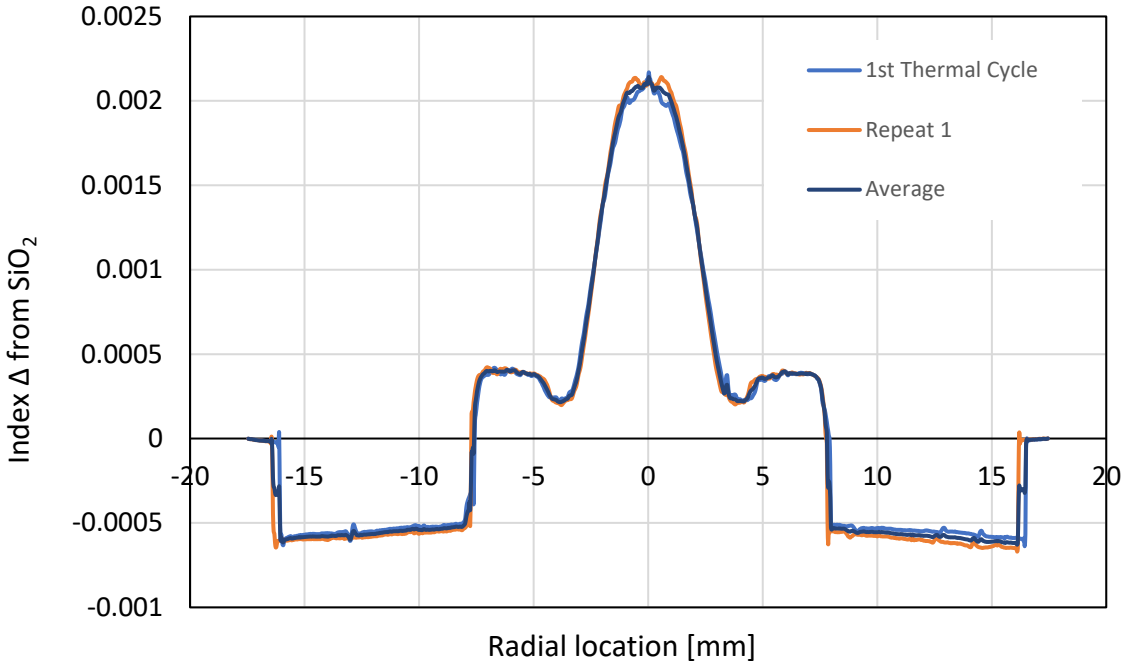

Figure 12: Each gradient index measurement was repeated and averaged to ensure accuracy.

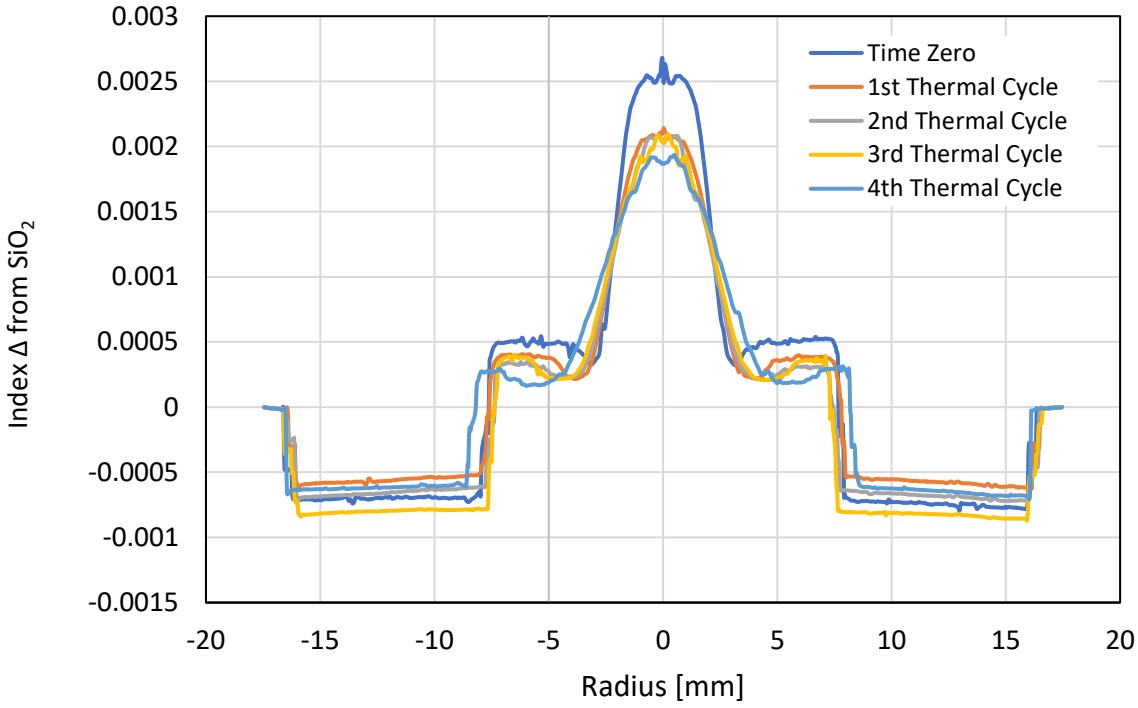

Figure 13: The gradient index profiles for the cane at time zero and after each thermal cycle.

The cane's geometry changed slightly throughout the thermal cycling process. The diameter increased in the middle of the cane, but the diameter decreased at the ends where the cane attached to the pure silica end caps. These changes are especially evident in the fourth thermal cycle data shown in Figure 13. Two possible causes are the potassium in the core diffusing outward or water from the hydrogen-oxygen burner diffusing into the glass from the cane's surface. Both potassium and water lower glass viscosity. The further the potassium diffused outward, or the water diffused inward, the lower the cane's viscosity. By the fourth thermal cycle, the viscosity was low enough for the surface tension to change the shape of the cane. Since the pure silica end caps contained no potassium, they had higher viscosity and resisted the pull of surface tension. This caused the ends of the cane to reduce in diameter and the middle to increase.

To account for this change in diameter, the data was normalized on radius. Figure 14 shows the gradient index profiles with normalized axes. The zero value on the x-axis is the center of the cane; the one value is the outside surface of the cane.

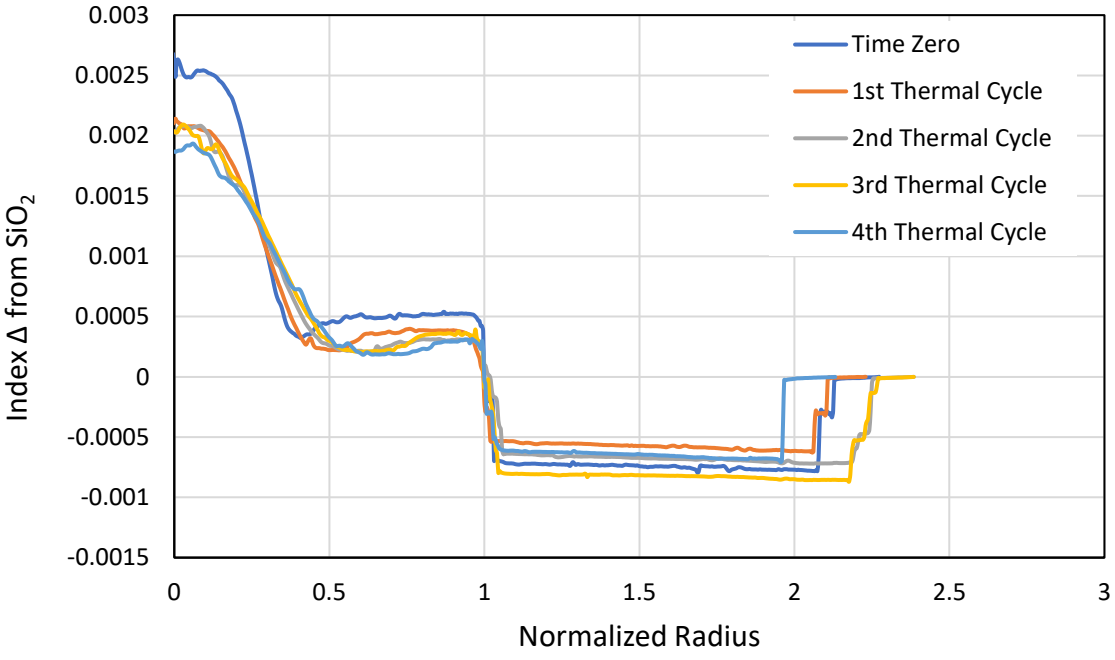

Figure 14: The gradient index profiles normalized to radius to eliminate variability in cane diameter.

G. SEM Collection

A scanning electron microscope (JSM-6010PLUS/LA) equipped with energy-dispersive x-ray (EDX) capabilities was used to analyze a cane.

The scanning electron microscope (SEM) and EDX were used to provide a second characterization method to support the index profile. The SEM was used to see if the potassium-doped core would be visible in back-scatter mode. The EDX was used to see if the potassium-doped core trended with the gradient index profile.

A cane that had not been heated was broken into a 1.5cm-long piece so it could fit inside the SEM. Before being placed inside the SEM, the piece of cane was observed under a polarized lens. Figure 15 shows the cane under the polarized lens, revealing the axial and radial stress in the glass due to the potassium-doped core. This inspection of axial stress was done before and after breaking the cane to ensure no stress changed occurred because of the fracture. The radial stress could only be viewed post-fracture.

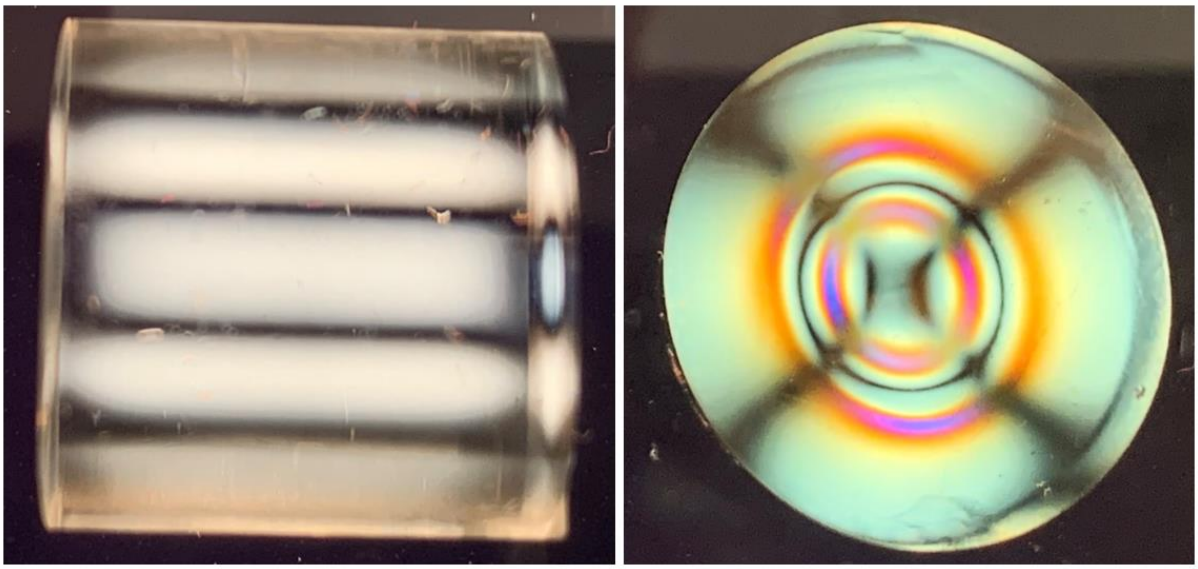

Figure 15: The glass cane through a polarized lens. Left: The axial stress due the chemical difference in the core is visible. Right: the radial stress in the cane.

The core-cladding interface can easily be seen with the eye (left image in Figure 16), but not in the SEM. Therefore, carbon conductance tape was laid over the core, with black dots marking the center and the edges of the core (right image in Figure 16). These marks acted as reference points in the SEM (Figure 17) to ensure the correct locations were analyzed.

Figure 16: Sample preparation for the SEM. Left: The core-cladding interface can be seen from an angle but not in the SEM. Right: Black dots at the edges and center of the core acted as reference points in the SEM.

Figure 17 shows how the black dots appeared in the SEM, and Figure 18 shows how the marks appeared on a carbon map from the EDX. The core was larger than the spot size of the EDX, so two images were taken to capture the entire core.

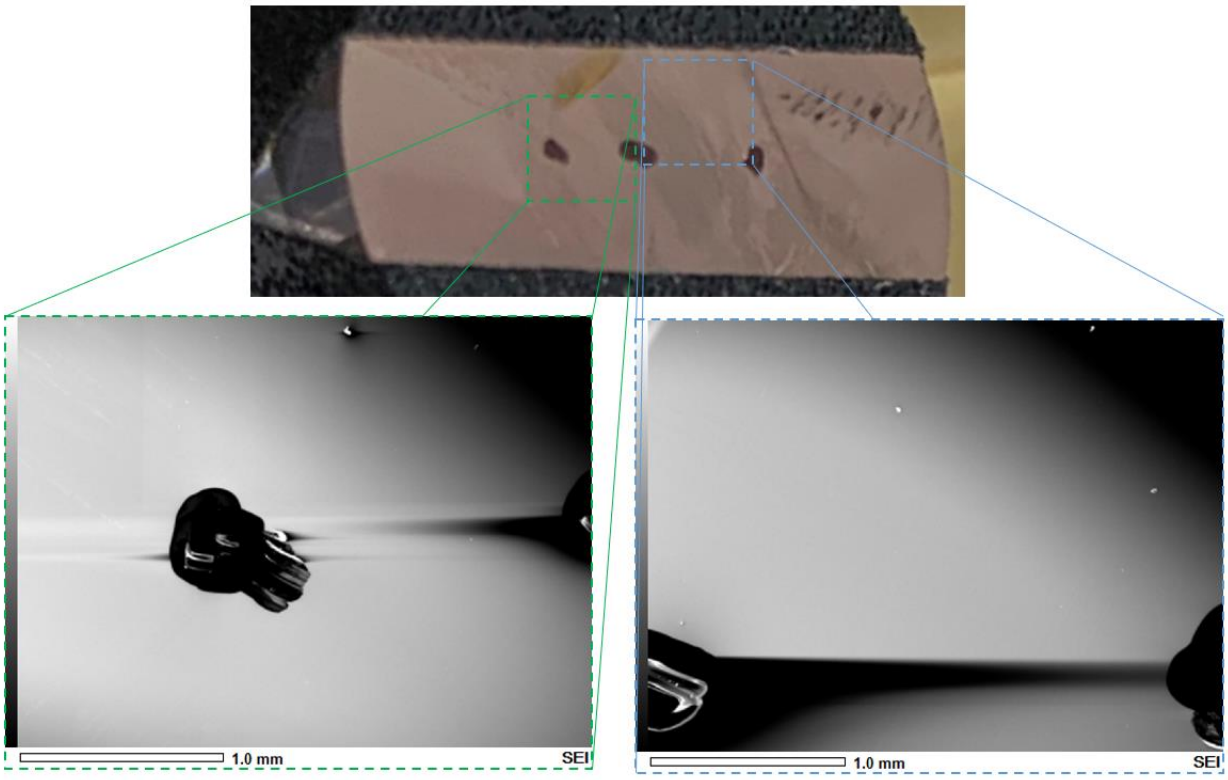

Figure 17: The marks under the SEM.

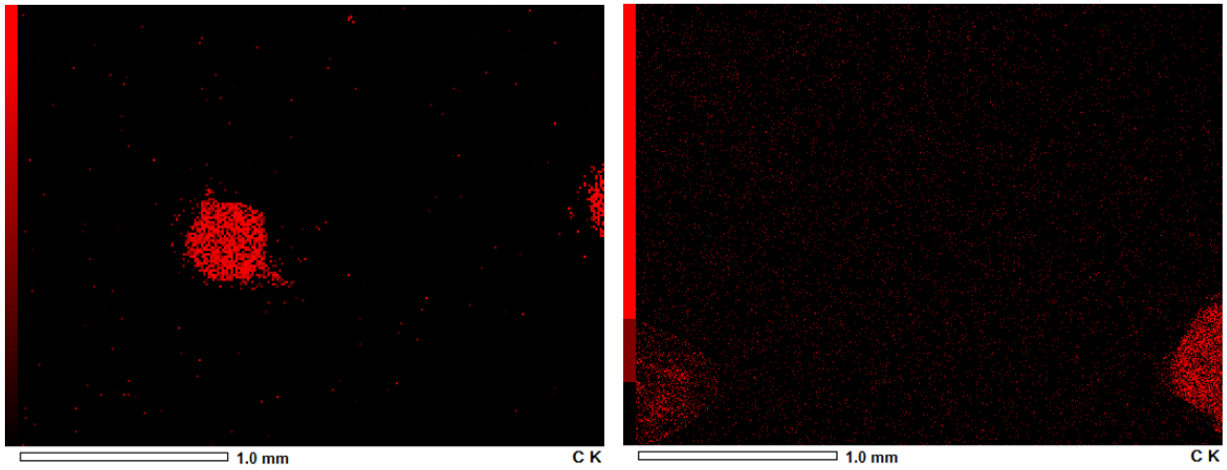

Figure 18: The marks on a carbon map from the EDX.

The two potassium maps in Figure 19 were taken at the same locations as the images in Figure 17 and Figure 18. These qualitative maps from the EDX showed an increase in potassium across the core, supporting gradient index data.

The EDX showed no alkalis or index modifiers other than potassium, which supports the assumption that the increase in gradient index is solely from the potassium. This characterization is sufficient because the canes contained only one alkali. (If more than one alkali was used to dope the cane or quantitative data was necessary, a micro-probe analyzer could provide further characterization.)

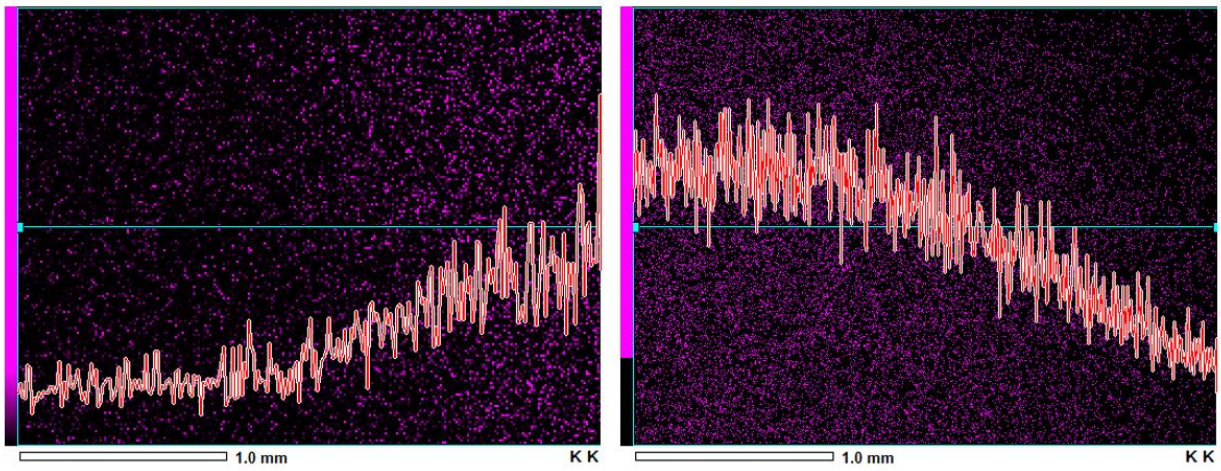

Figure 19: A potassium map from the EDX shows an increase in potassium across the core, supporting gradient index data.

H. Gradient Index to Mol% K_2O Calculation

The next step was to use the gradient index data to calculate total alkali concentration, which required converting the refractive index data to a mol%. The term refractive index is used to describe the index of refraction at a single point, whereas the term gradient index is used to describe the collection of refractive index data points across a cane.

A literature search on the effects of potassium in glass led to research by Lines [16], who provided refractive index data for different concentrations of potassium in silica glass from Schroeder [17] and Bansal and Doremus [18]. The first two columns in Table III and Table IV list the potassium concentration to its corresponding refractive index data needed for this analysis. The third column lists the index delta ratio, which normalizes the data and was calculated using Equation *2*.

Equation 2 $$Index\ Delta\ Ratio = \frac{n_{SiO2}(\lambda) - n_{xK2O+(100-x)SiO2}(\lambda)}{n_{SiO2}(\lambda)}$$

Table III: Refractive Index for Different Concentrations of Potassium-Silicate Glass at T=296K, λ=6328.1Å from Schroeder[17].

K_2O/SiO_2 [mol %]	n(6328 Å)	Index Delta Ratio
0/100	1.4577	0.0000
6/ 94	1.46783	0.0069
8/ 92	1.47152	0.0095
10/ 90	1.47483	0.0117
15/ 85	1.48423	0.0182
20/ 80	1.49239	0.0238
25/ 75	1.49752	0.0273
33/ 67	1.50498	0.0324
38/ 62	1.51048	0.0362
40/ 60	1.5111	0.0366

Table IV: Refractive Index for Different Concentrations of Potassium-Silicate Glass at T=296K from Bansal and Doremus[18].

Composition [mol % K_2O]	n_D(5893 Å)	Index Delta Ratio
0/100	1.4584	0.0000
10.00	1.4800	0.0148
15.00	1.4867	0.0194
20.00	1.4937	0.0242
25.00	1.4995	0.0282
30.00	1.5048	0.0318
35.00	1.5093	0.0349
40.00	1.5136	0.0378
45.00	1.5175	0.0405

The graph in Figure 20 plots the data from Table III and Table IV. The data is asymptotic, shifting to a new constant as the concentration of potassium increases. However, because the present 1.2mol% K_2O canes contained a very small amount of potassium, it was necessary to use a local linearity approach and only analyze data less than 20mol% K_2O, as shown in Figure 21. Now both sets of data are in close agreement, having identical slopes with only slight offsets in y-intercepts.

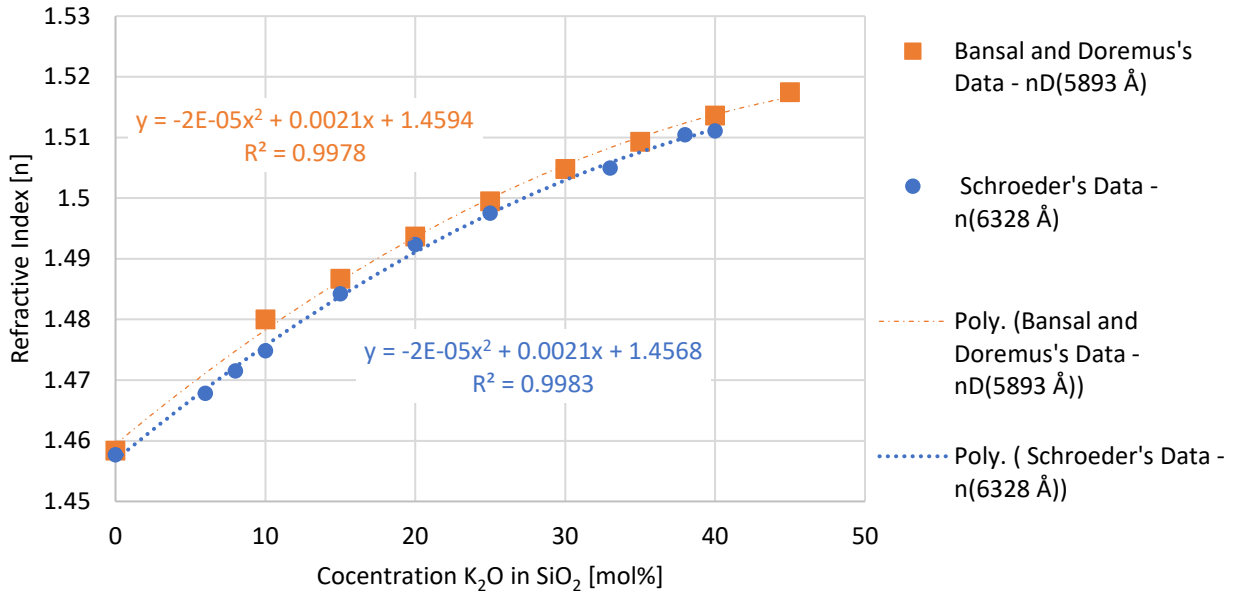

Figure 20: Bansal and Schroeder's data show how increasing the concentration of potassium in pure silica affects the refractive index.

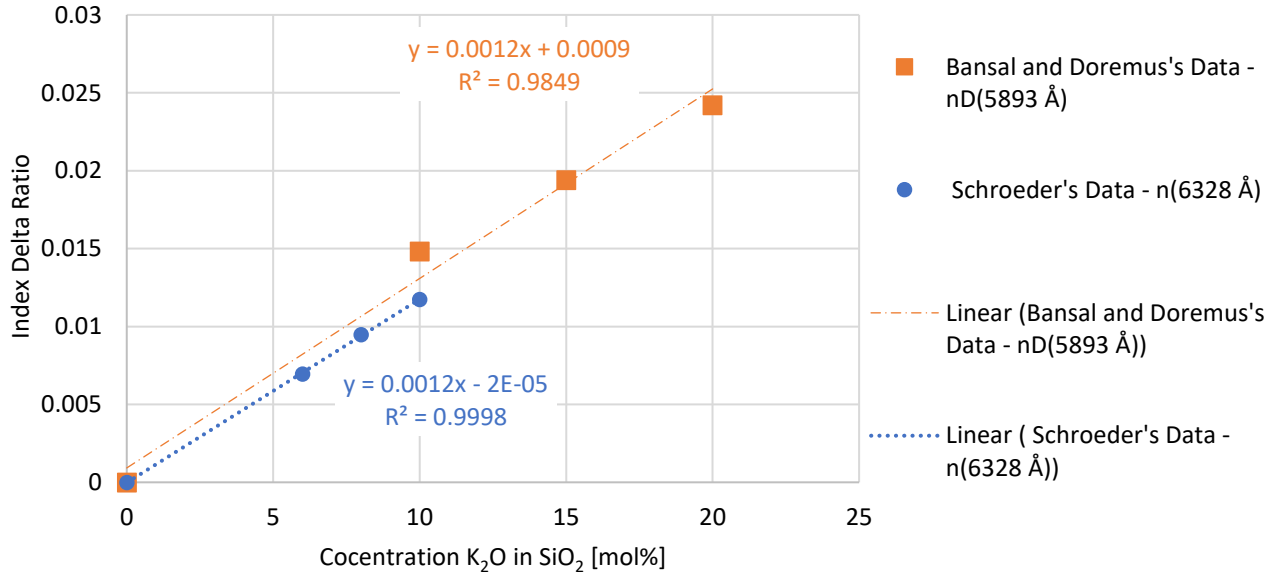

Figure 21: Normalized index delta data with a local linearity on data less than 20mol% K_2O. The K_2O Index Δ value is given by the slopes which are 0.0012.

This local linearity approach simplifies determining the relationship constant called the K_2O Index Δ, which is equal to the slope of the lines 0.0012 (with units Index Delta Ratio/mol% K_2O) in Figure 21. Plugging this value into Equation *3* will determine the mol% of potassium oxide.

Equation 3

$$mol\%\ K_2O = \frac{\left(\frac{n_\Delta}{n(\lambda)_{SiO_2}}\right) - n_{correction}}{K_2O\ Index\Delta}$$

Equation *3* normalizes the raw data with the laser wavelength λ. The laser wavelength of the P106 preform analyzer is 1550nm, and the pure silica cell is n_{SiO2} = 1.44402345426.

The correction factor ($n_{correction}$) can set the raw glass chemistry to a zero value. The correction factor was found by averaging the gradient index data for the cladding portion of each cane. This is because it is unlikely that potassium increased the index of refraction in the cladding (see Table II). The base glass is set to zero because the goal is to determine the total potassium concentration from the increase in gradient index across the core of the cane. (This concentration will be used later with an area under the curve method.)

Figure 22 illustrates the correction factor. It shows the cane at Time Zero and the raw data for the base glass with an index delta slightly above silica. The correction factor shifts the gradient index down, reducing the base glass to zero. Now any increase in the gradient index will be a result of only the added potassium.

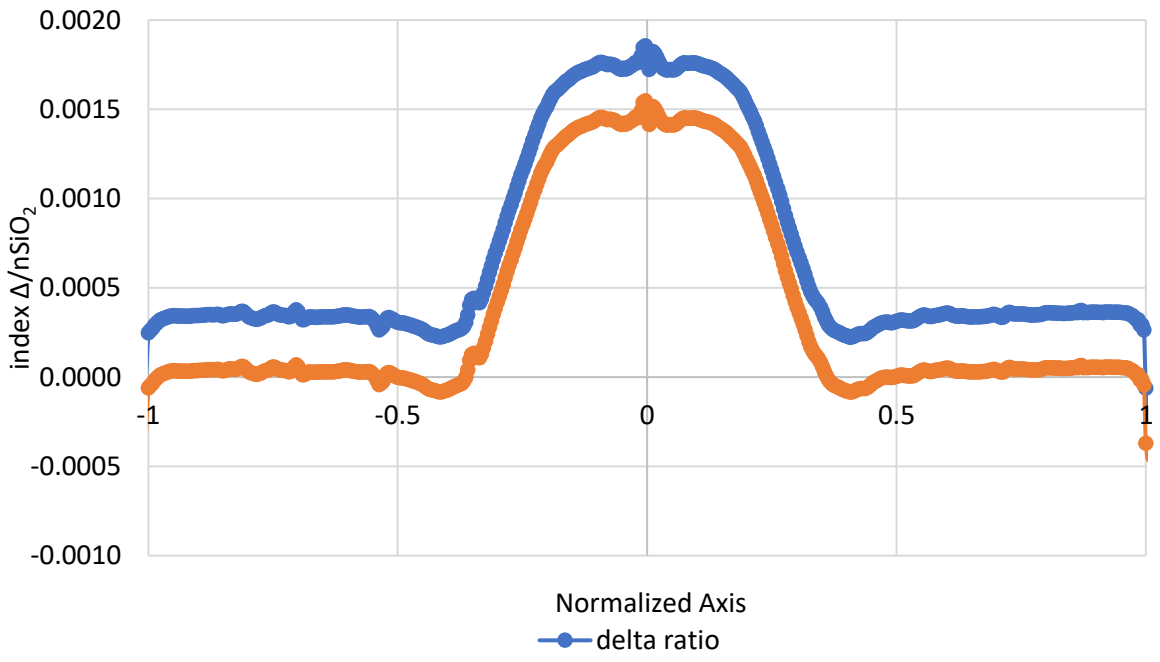

Figure 22: The raw data has a delta slightly above silica. The base glass is corrected to zero so the increase in gradient index in the core is a result of added potassium.

Figure 23 shows all the gradient index profiles from Figure 14, corrected to make the gradient index of the cladding equal to pure silica.

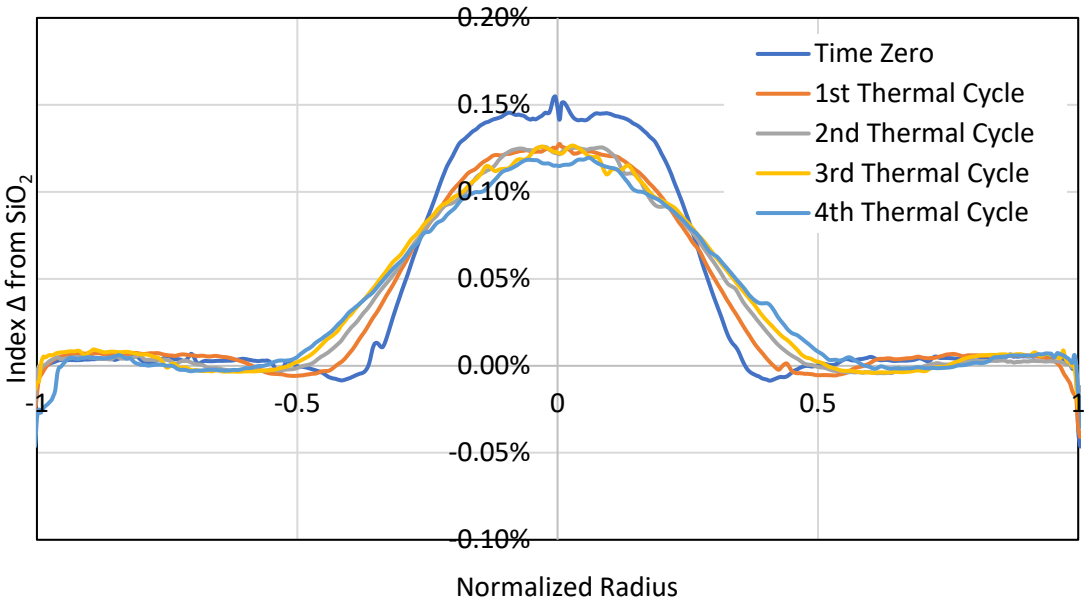

Figure 23: All the gradient index profiles corrected to zero for pure silica base glass.

Continuing with Equation *3*, using the determined value of 0.0012 K_2O Index Δ with units of refractive index delta ratio over mol% K_2O, resulted in a concentration of K_2O in mol% radially across the cane. Each gradient index profile can now be plotted in mol% K_2O. Figure 24 shows the potassium diffusion extent at Time Zero is 2.79 mm, measured radially through the core of the cane.

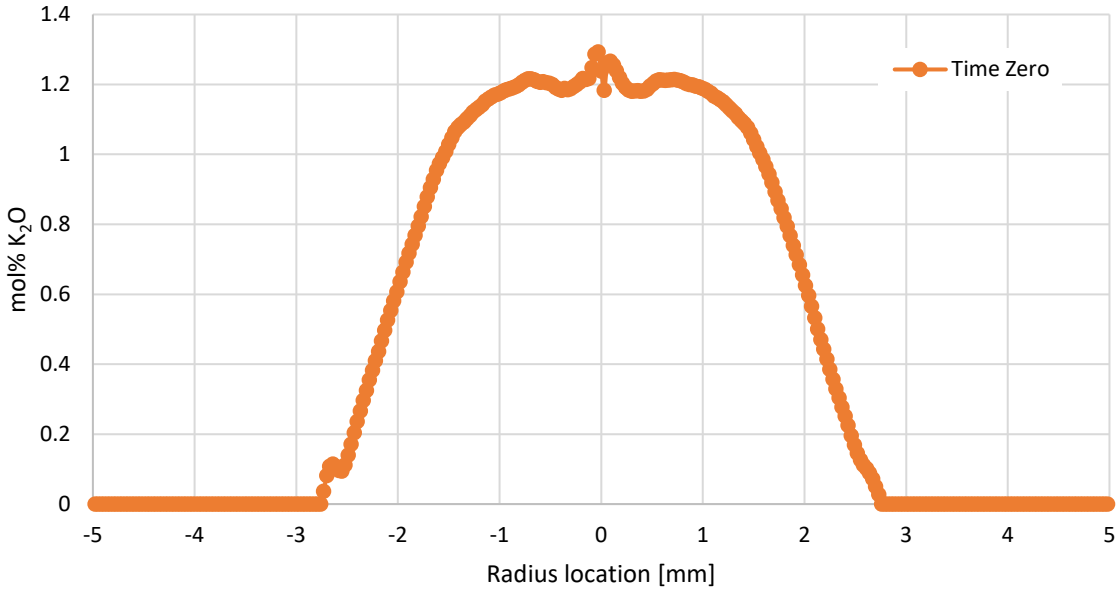

Figure 24: The mol% K_2O radially through the core of the cane at Time Zero.

This value can be converted to wt% K_2O. Figure 25 shows the cane had a peak of 2wt% K_2O at Time Zero.

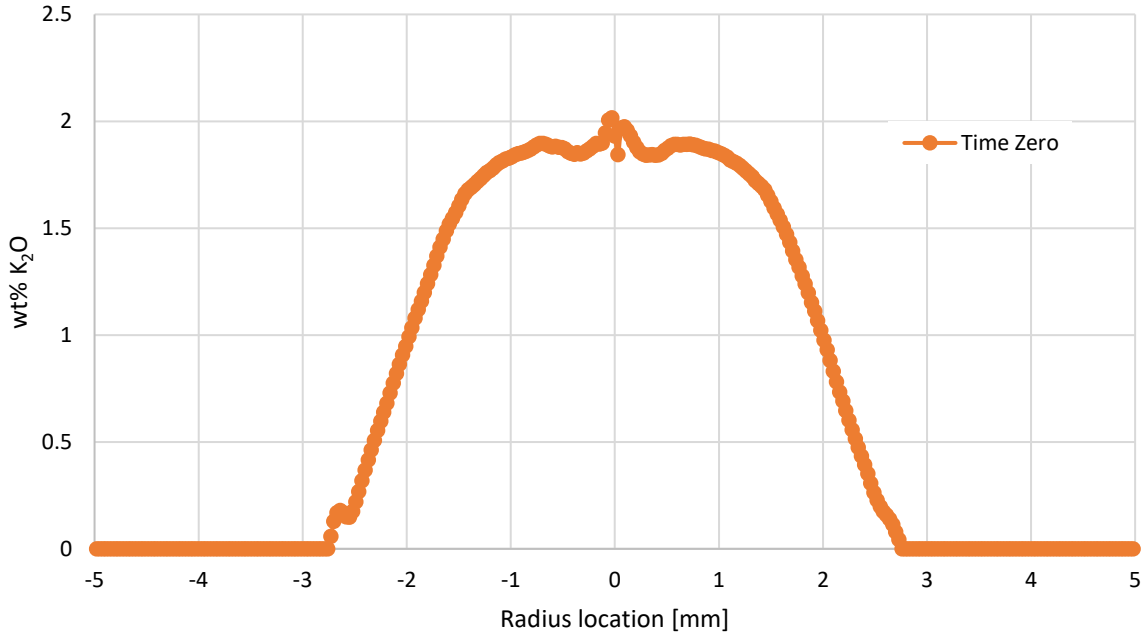

Figure 25: The wt% K_2O radially through the core of the cane at Time Zero.

III. ANALYSIS AND DISCUSSION

The Arrhenius equation (Equation *12*) shows that diffusion coefficients are highly temperature dependent. Furthermore, at these elevated temperatures other possible rate-controlling processes may be larger than anticipated. The IVD process conducted to diffuse K^+ into the silica network requires the presence of a charge-balancing anion. Thus, OH, O^-, or O_2 must migrate with the potassium to form K_2O in the glass. Therefore, multiple factors must be considered, including oxygen (O_2) diffusion, OH diffusion from the burner at the glass surface, the viscosity rate diffusion at elevated temperatures, and the combination of viscosity and water controlling the diffusion rate.

A. Diffusion Distance with Gradient Index Profiles

As described above, the gradient index data was converted to mol% K_2O, and the radial axis was normalized to accurately analyze diffusion. This data is shown in Figure 26, Figure 27, and Figure 28.

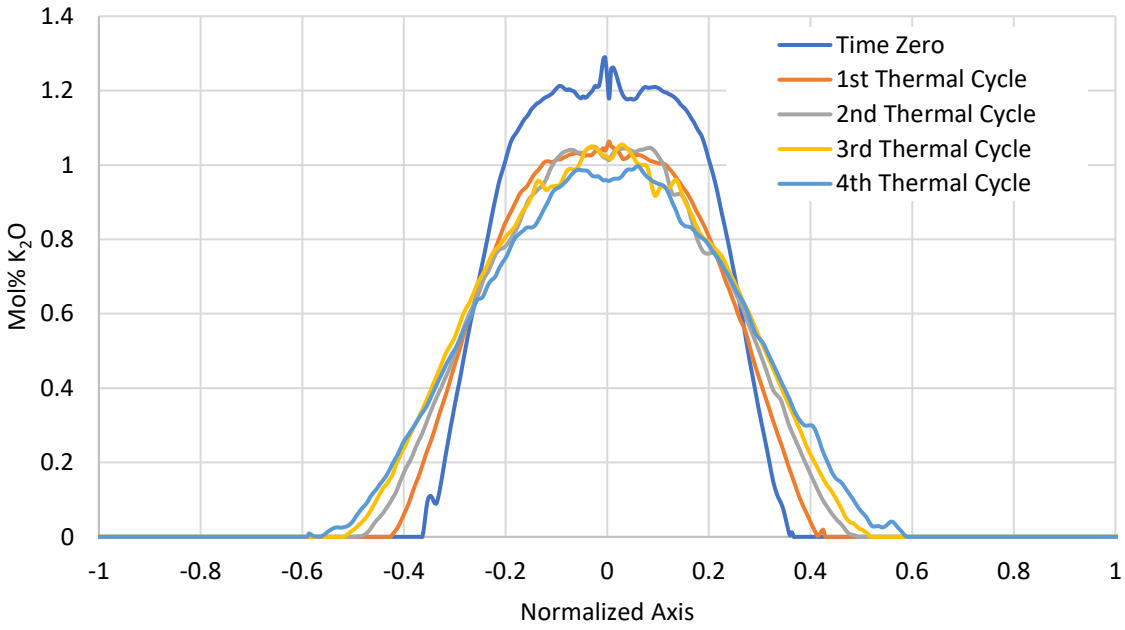

Figure 26: The gradient index data for all thermal cycles converted to mol% K_2O normalized radially across the core of the cane.

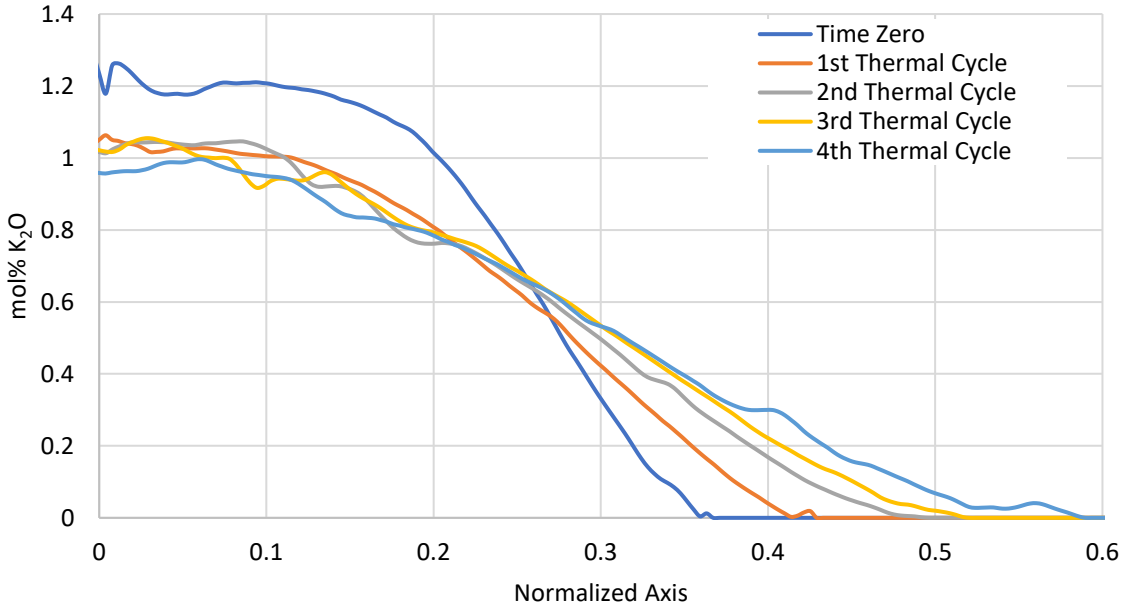

Figure 27: The gradient index data for all thermal cycles converted to mol% K_2O normalized radially across the cane, localized to one side of the core.

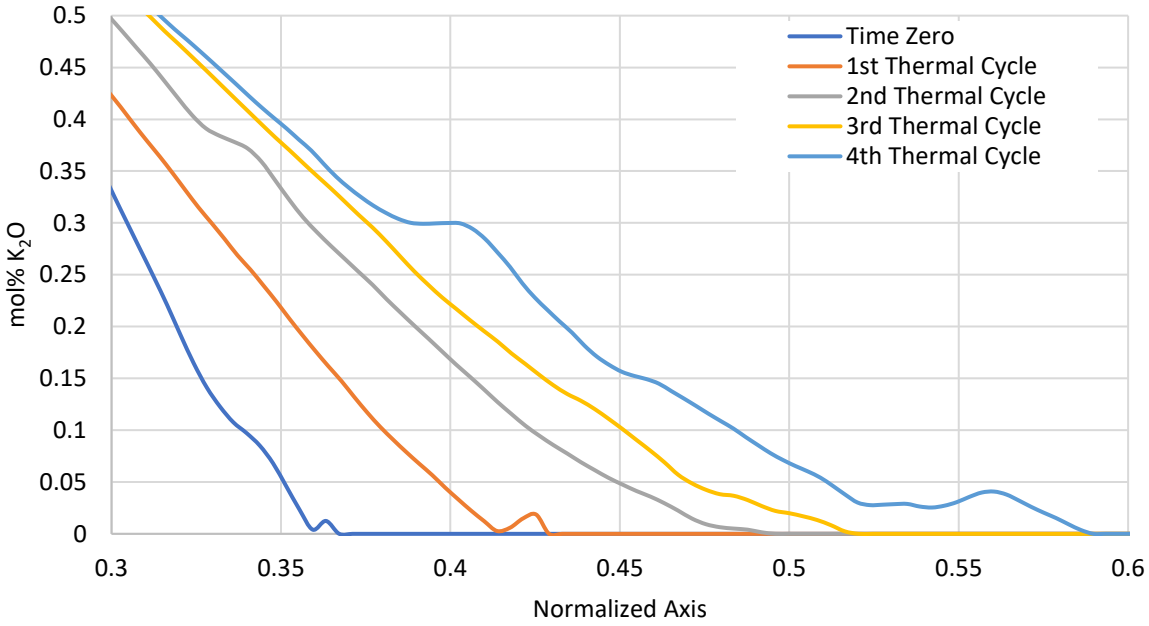

Figure 28: Magnification from Figure 27 the gradient index data for all thermal cycles converted to mol% K_2O normalized radially across the cane, localized to the potassium diffusion extent.

Figure 27 and Figure 28 most clearly show the potassium diffusion distance. At Time Zero, potassium was at radial position 36.7% of the normalized axis, and by the end of the fourth thermal cycle the potassium had moved more than halfway across the radius of the cane, ending at 59.0%.

To calculate the radial diffusion distance between thermal cycles, the normalized potassium extents were multiplied by the initial cane diameter of 15.27mm. This data is shown in Table V for both the left and right sides of the gradient index profiles. The average is the diffusion distance.

Table V: The Potassium Diffusion Extent as Measured Between Each Thermal Cycle, Normalized with Initial Radius at Time Zero.

Thermal Cycle	**K extent Left side [Normalized]**	**K extent Left side [mm]**	**K extent Right side [Normalized]**	**K extent Right side [mm]**	**K extent Average [mm]**
Time 0	-0.3636	-2.78	0.3672	2.80	2.79
1st TC	-0.4269	-3.26	0.4291	3.28	3.27
2nd TC	-0.4939	-3.77	0.4918	3.75	3.78
3rd TC	-0.5185	-3.96	0.5205	3.97	3.97
4th TC	-0.5901	-4.51	0.5897	4.50	4.50

Table VI shows the potassium diffusion distance for each thermal cycle. The third thermal cycle appears to be an outlier, with a diffusion distance about half as long as the other three cycles.

Table VI: The Potassium Diffusion Distance for Each Thermal Cycle.

Thermal Cycle	Diffusion distance for each thermal cycle [mm]
Time 0	0
1st TC	0.48
2nd TC	0.51
3rd TC	0.19
4th TC	0.54

B. Time and Temperature

Several works by Kirchhof [7]-[12] outline a method of using the thermal profile of a traversing heat source to determine an equivalent temperature for diffusion coefficients. Equation *4* relates the thermal profile maximum temperature for a traversing heat source to this equivalent temperature T_e. The equivalent temperature is based on the activation energy of the diffusion species to provide an accurate temperature for diffusion over an axial length Δz_B defined as the width of the thermal profile at T_e.

Equation 4
$$\frac{1}{T_e} = \frac{1}{T_{max}} + \frac{R}{E_A}$$

Where E_A is the activation energy, R is the ideal gas constant, and T_{max} is the peak temperature at the surface. The activation energy for potassium was determined with the Anderson-Stuart model (A-S) [19]– [23] where the jump distance λ was used as suggested by McElfresh and Howitt [24].

Equation *5* is the activation enthalpy of diffusion defined by the sum of the binding energy and the strain energy.

Equation 5
$$E_A = \frac{k\beta z z_0 e^2}{\varepsilon(r_K + r_O)} + 4\pi G\lambda(r_K - r_D)^2$$

Where k is coulombic potential; β is the finite displacement factor; z and z_0 are the valences of the mobile ion pair, in this case the Pauling ionic radius of potassium and oxygen r_K and r_O respectively; r_D is the size of the doorway; e is the electronic charge; ε is the dielectric permittivity; and G the elastic modulus.

Equation *6* is the finite displacement factor β from the A-S model with constants a=2.1 and b=3.5 angstroms.

Equation 6
$$\beta = \frac{a - r_K}{b}$$

The activation energy is dependent on the concentration n in mol% in both the dielectric permittivity ε (Equation 7) and the elastic modulus G (Equation *8*).

Equation 7 $$\varepsilon = \varepsilon_0 - \frac{d\varepsilon}{dn}n$$

Equation 8 $$G = G_0 - \frac{dG}{dn}n$$

The A-S model for the present 1.2mol% K_2O cane from Equation *5* provided an activation energy 1.18 eV/atom (114kJ/mol). This data appears to be consistent with other studies [19]– [24] and with the data for alkali metals in silica systems measured by Charles [25] plotted in Figure 29.

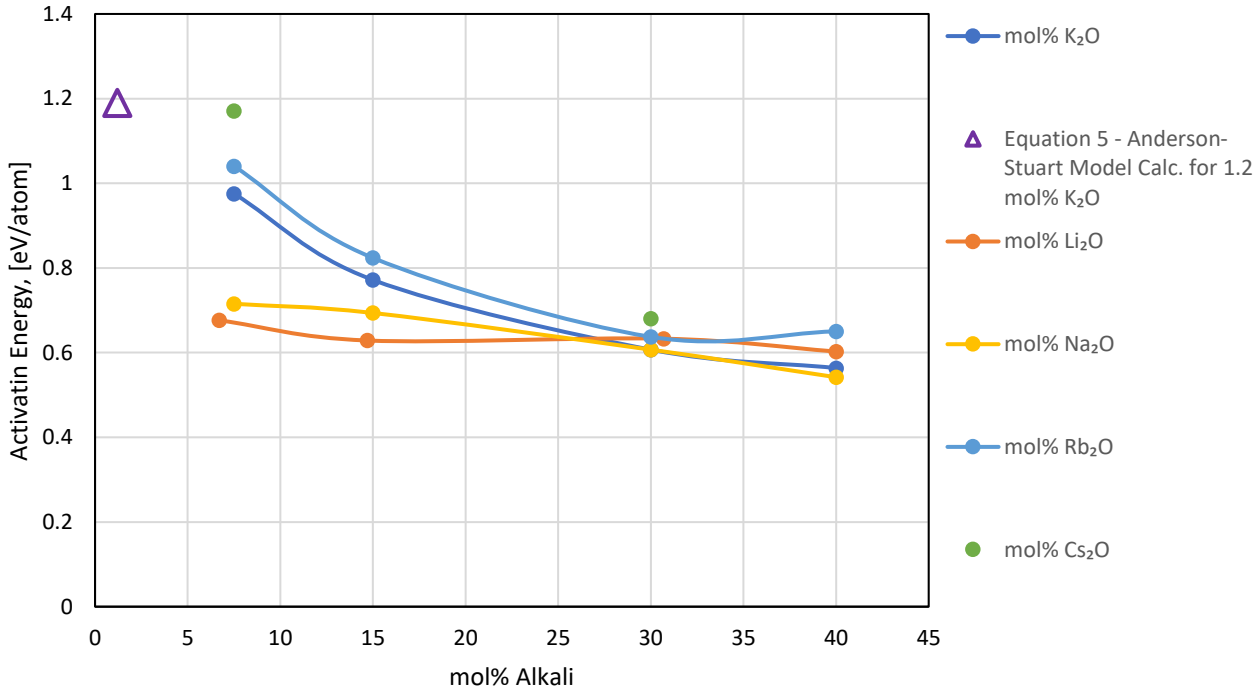

Figure 29: The activation enthalpy of alkali ions as a function of concentration. Comparing data from Charles [25] to Equation 5.

With a known activation energy, Equation *4* can be used to determine the equivalent temperature for diffusion. However, the max temperature was cut short from the thermal profile due to the camera limits (Figure 10). To extrapolate a maximum temperature, a polynomial best-fit function can continue the parabolic profile. Figure 30 shows the extrapolated curve for the max temperature of 2256°C along with the results for the equivalent temperature using Equation *4*.

The infrared camera profile was used with Equation *4* because of a suspected error in the pyrometer measurements. There was a significant difference between the thermal camera and the pyrometer data: the thermal camera extrapolated out to 2256°C while the pyrometer measured 2180°C. Both instruments are of high quality, and great care was taken during setup. But when

measuring the curve of a small cane with a comparatively large spot size, small discrepancies are expected.

Equation *4* gave an equivalent diffusion temperature of 1865°C. The effective axial width ΔZ_B is defined by the length across the thermal profile at the equivalent temperature. In Figure 30 the axial width is 63.0mm.

Equation *9* from Kirchoff [9] calculates the time for diffusion t_D.

Equation 9
$$t_D = n\left(\frac{\Delta z_B}{v_B}\right)$$

Where n is the number of burner passes, ΔZ_B is the effective axial width, and v_B is the burner traverse velocity. The effective axial width can be solved for using the thermal profile in Figure 30 with the equivalent temperature of 1865°C. Each thermal cycle was a single burner pass with a constant velocity of v_B = 2mm/min resulting in a diffusion time of t_D = 31.5 min.

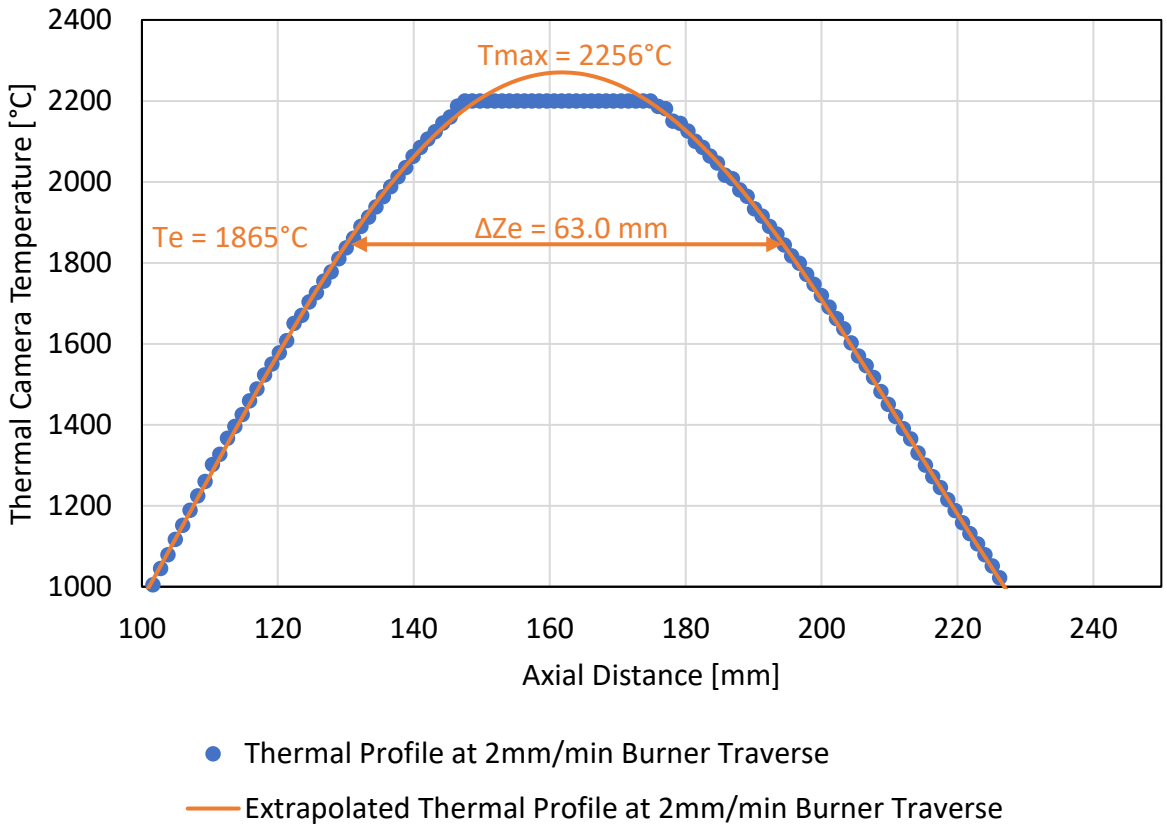

Figure 30: The thermal profile of a burner pass. Using Kirchhof's [7]-[12] method for equivalent diffusion temperatures, the ΔZ length was calculated to be 63.0mm.

C. Diffusion Coefficient

Several methods have been used to model diffusion. Brownian motion was named after Robert Brown, who used a microscope to observe pollen moving sporadically when suspended in water

[26]. Brownian motion, sometimes referred to as random jump theory, has been modeled with Fick's First and Second laws. Mehrer [26] has a derivation of Fick's laws and applied this method to crystalline solids, while Varshneya [27] applied it to glasses.

Diffusion in its simplest form is a one-directional model of flux. Varshneya provides a derivation for flux J in Equation 10, where r is the average jump distance and ν is the frequency of jumps.

Equation 10 $$J = -\frac{1}{2} r^2 \nu \frac{dc}{dx}$$

Equation *11* combines Equation 10 with Fick's First Law. It provides an expression for the diffusion coefficient as particles moving through an area over time [27].

Equation 11 $$D = \frac{1}{2} r^2 \nu$$

Equation *11* and the total potassium diffusion distance in Table VII were used to determine a diffusion coefficient after each thermal cycle. It is important to note that the diffusion coefficient of potassium (D) in Table VII came from the present 1.2mol% K_2O experiment. These values differ from the pre-exponential value (D_0), a constant value from the Arrhenius equation, Equation *12*. The diffusion coefficient was previously mentioned in Table I.

Equation 12 $$D = D_0 e^{\left(\frac{-E}{RT}\right)}$$

The pre-exponential constant D_0 was solved for with activation energy from Equation *5* and the diffusion coefficient value from Equation *11*. The results are in Table VII.

Table VII: The Time for Diffusion at the Equivalent Temperature 1865°C, the Diffusion coefficient D, the pre-exponential constant D_0, and the Diffusion Distance for Each Thermal Cycle.

Thermal Cycle	t_D at Te 1865°C [min]	D [cm^2/s]	D_O [cm^2/s]	Diffusion Distance [mm]
1st TC	31.5	5.91×10^{-7}	3.78×10^{-4}	0.47
2nd TC	63	1.20×10^{-6}	7.66×10^{-4}	0.95
3rd TC	94.5	1.21×10^{-6}	7.73×10^{-4}	1.17
4th TC	126	1.91×10^{-6}	1.22×10^{-3}	1.70

The average diffusion coefficient for a peak of ~1.2mol% potassium oxide concentration to diffuse into silica glass when exposed to a temperature of 1856°C was D = 1.23 x 10^{-6} cm^2/second with a standard deviation 0.54 x 10^{-6} cm^2/second. The average pre-exponential constant was D_0 = 7.84 x 10^{-4} cm^2/second with a standard deviation of 3.45 x 10^{-4} cm^2/second.

This diffusion coefficient is consistent with the diffusion coefficient of Rothman [2] (see Table I), but Rothman used much colder temperatures. Tamura [1] used high temperatures, and their diffusion coefficient is slightly greater than the present findings. Tamura's glass contained fluorine, which would cause faster diffusion rates. Unfortunately, their explanations are vague because their work was patented.

To understand what may be driving the diffusion rate at these elevated temperatures, some analysis was done to compare the present 1.2mol% K_2O diffusion rate to models for viscosity-driven diffusion, oxygen diffusion, and water diffusion.

First, a model was used to determine the viscosity of the glass cane. Data compiled from different weight percentages of potassium were plotted and linear fit to provide the most accurate slope for a 1.2mol% K_2O in pure silica. Figure 31 shows this plot, along with data from Bockris et al. [28] and Doremus [30]. The square marker is the viscosity of the cladding at the surface temperature of 2256°C. The triangle marker is the viscosity of the core at 1865°C.

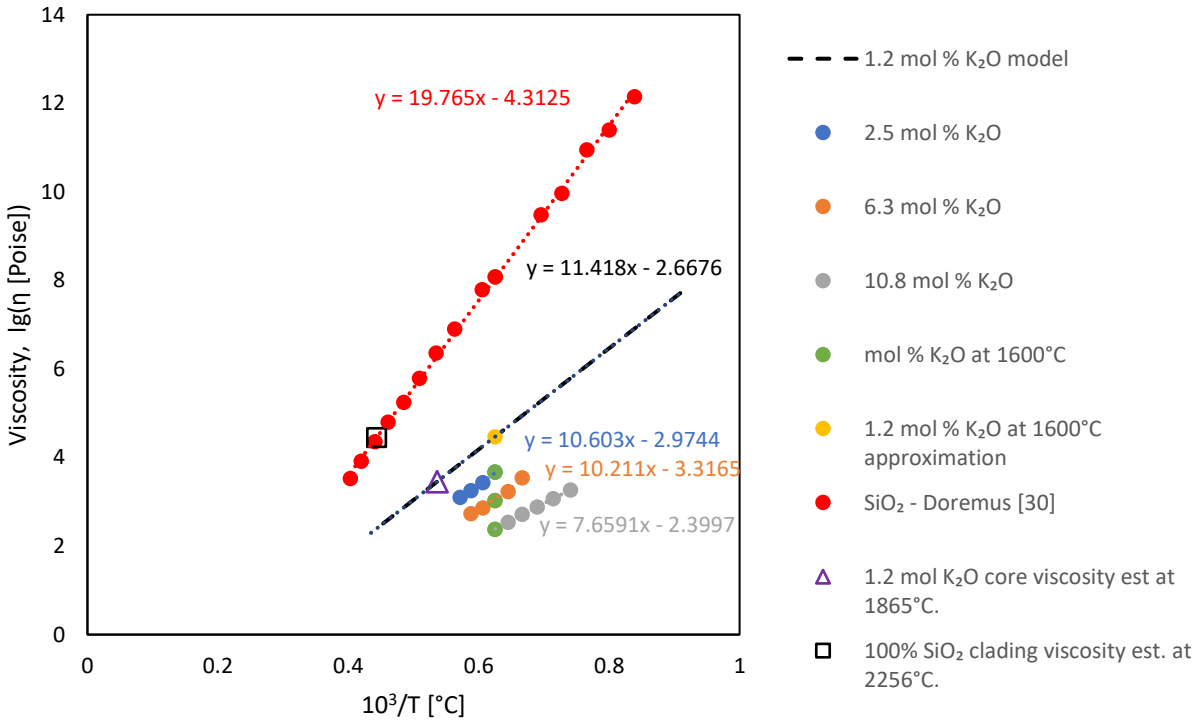

Figure 31: The viscosity data for pure silica from Doremus [30] and potassium silica data from Bockris et al. [28] was used to determine a viscosity curve for 1.2mol% K_2O.

The data in Figure 31 can be used to estimate a viscosity value for the entire temperature span by applying Equation 13, the Stokes-Einstein model for diffusion [27][31].

Equation 13 $$D = \frac{k_B T}{B r \eta}$$

Figure 32 shows all the diffusion coefficient models discussed in this work, for comparison purposes: the Stokes-Einstein model, the data from the present 1.2mol% K_2O experiment and its Arrhenius model, potassium diffusion data from Smith [4], Rothman [2] and Tamura [1], oxygen diffusion data by Berezhnoi and Boiko [32] and its Arrhenius model, and water diffusion data by Scholze [33], [29], and an Arrhenius model of OH diffusion in silica by Kirchhof [11].

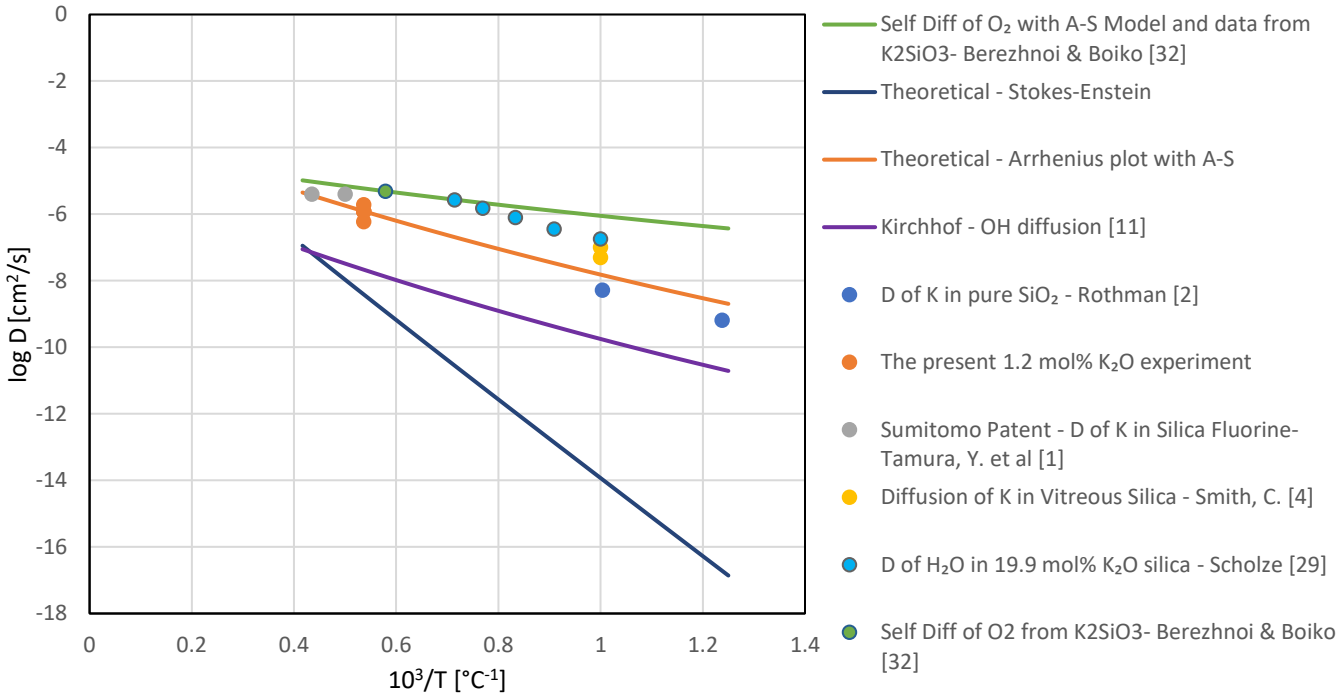

Figure 32: The present 1.2mol% K_2O potassium diffusion data compared to data from Smith [4], Rothman [2] and Tamura[1], along with the theoretical Stokes-Einstein model from Equation 13, oxygen diffusion data by Berezhnoi and Boiko[32], and water diffusion from Scholze [33], [29].

Each of the works on potassium diffusion shown in Figure 32 merit discussion.

The diffusion rate published by Tamura [1] is in good agreement with the diffusion rate determined here with the present 1.2mol% K_2O concentration. Tamura's diffusion is slightly faster because of the fluorine in their glass and perhaps a slightly greater concentration of K_2O.

When compared at similar temperatures, Smith's data is slightly elevated above from that of Rothman [2]. However, an Arrhenius model of the present 1.2mol% K_2O data agrees well with Rothman's data.

The Stokes-Einstein model for viscosity rate driven diffusion does not appear to support any of the potassium diffusion rates here. Work by Avramov [31] shows that the diffusion rates of

small, faster-moving particles such as alkali metals do not follow the Stokes-Einstein model. The diffusion coefficients are not driven by viscosity; therefore Stokes-Einstein is not an accurate model for the present 1.2mol% K_2O experiment.

Because the present 1.2mol% K_2O diffusion data does not fit the viscosity model of diffusion, it was then compared with oxygen and water diffusion rates.

Berezhnoi & Boiko [32] studied oxygen diffusion in silica. While their data and the present 1.2mol% K_2O have similar magnitudes, the shallower slope of their Arrhenius model causes a larger separation from the 1.2mol% K_2O model at lower temperatures.

Data from Smith [4] if a line were connected to the present 1.2mol% K_2O data, the two sets would create a line with a slope very close to the oxygen diffusion rate line. This indicates that Smith's diffusion rate may have been oxygen diffusion driven. But these are very subtle differences between the data sets and hard to draw a definitive conclusion.

Scholze [33] [29] studied diffusion of water in potassium-silica glass. His diffusion rates have a greater magnitude than the present 1.2mol% K_2O, but the two slopes match. Scholze also had more potassium in the glass:19.9 mol% K_2O. When comparing Scholze to Kirchhoff's [11] data on OH diffusion with 0.0 mol% K_2O, the slopes are again consistent with water. But the small concentration of potassium has a large effect on the diffusion rate of water, just as small concentrations of potassium have large effects on the viscosity of silica.

This suggests that the potassium diffuses rate was accelerated by water in the glass. While there is only 30ppm of OH in Heraeus HSQ300 (Table II), the hydro-oxygen burner drives water onto the cane's surface, and this water diffuses into the glass. The distance the water diffuses can be calculated by using the line of best fit for the water-driven diffusion by Scholze [33] [29]. Extrapolating to our temperature of 1865°C for 126 minutes results in the water diffusing 4.60mm into the glass – a surprising outcome. The water probably went even further than that, because the water started at the surface where the temperature was estimated to be 2256°C and would have started driving inwards in the fabrication phases of sample preparation.

Figure 33 shows the relevant data from Figure 32 overlayed with diffusion rate models, labeled as oxygen-driven, water-driven and viscosity-driven. This makes it evident that the diffusion rate in the present 1.2mol% K_2O experiment was primarily water-driven, with an offset due to the concentration of potassium.

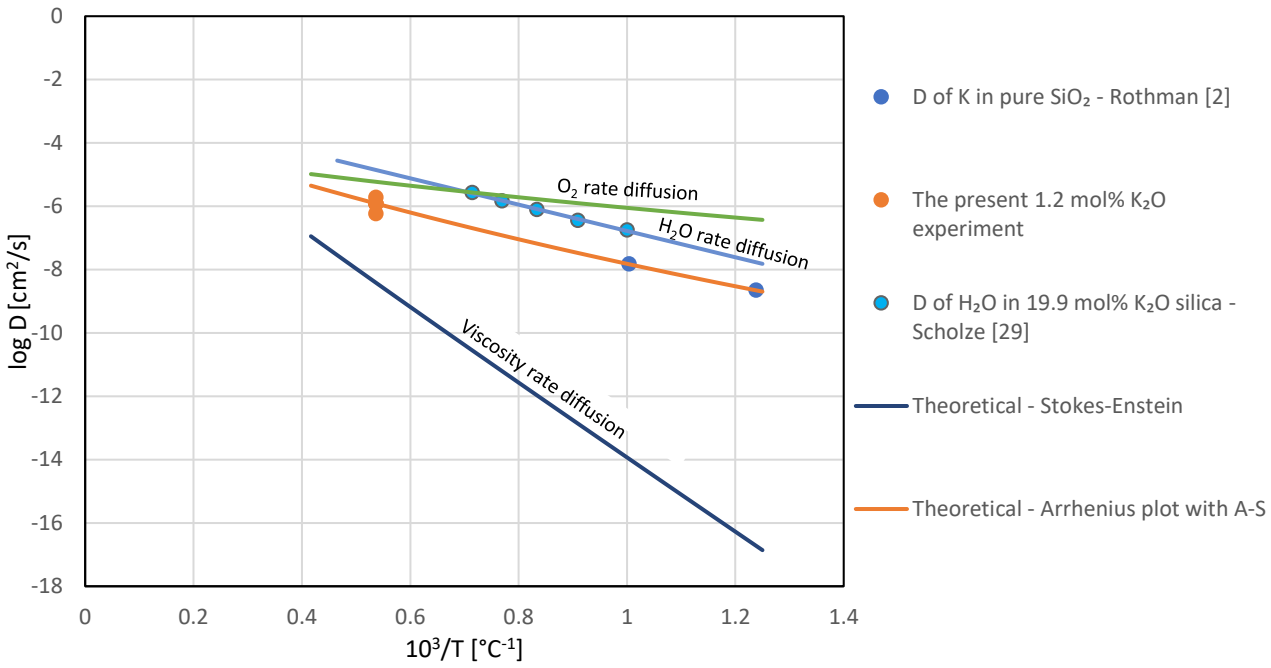

Figure 33: The diffusion rate models overlayed on the relevant data show that the diffusion rate of this experiment was driven by water, with an offset due to the potassium.

Furthermore, the concentration of potassium plays a large role in the diffusion rate of the OH, data from Kirchoff [11] shown in Figure 34. Kirchoff's data was left out of Figure 33 but in Figure 34 it is compared to the water diffusion rates, with varying levels of potassium concentration. It is evident that a small amount of potassium has large effects on the diffusion rate of water in silica.

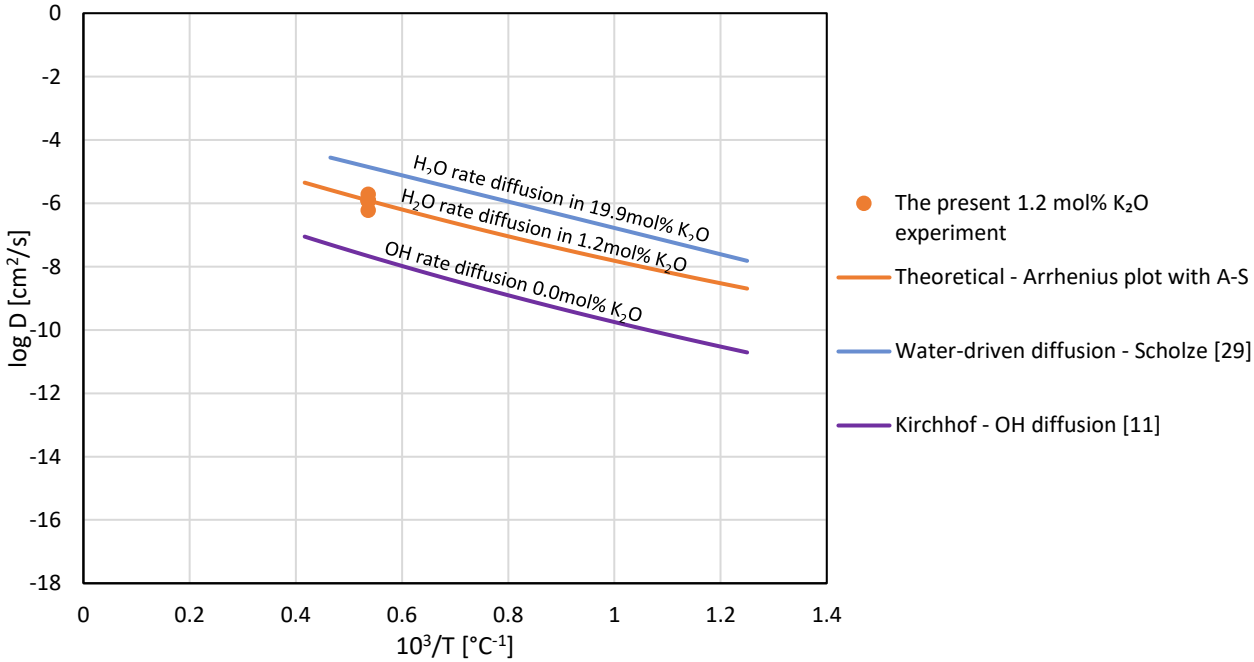

Figure 34: The diffusion rate models for water with varying levels of concentration of potassium

D. Suggestion for Future Work

To further test this theory and track where the alkali and the water meet, the present 1.2mol% K_2O experiment could be repeated with a longer cane. It is suggested to begin by measuring the gradient index in five locations down the length of the glass. Cut off the glass at the last measurement location to characterize, with electron probe microanalysis (EPMA) to find the radial concentration of the alkali. Use Fourier transform infrared spectroscopy (FTIR) to find the radial concentration of the OH. After a thermal cycle, measure the gradient index in four locations. Cut off the glass at the last location, and measure again with EPMA and FTIR. Repeat cycling, measuring, and analyzing the remaining locations. Figure 35 illustrates this proposed experiment.

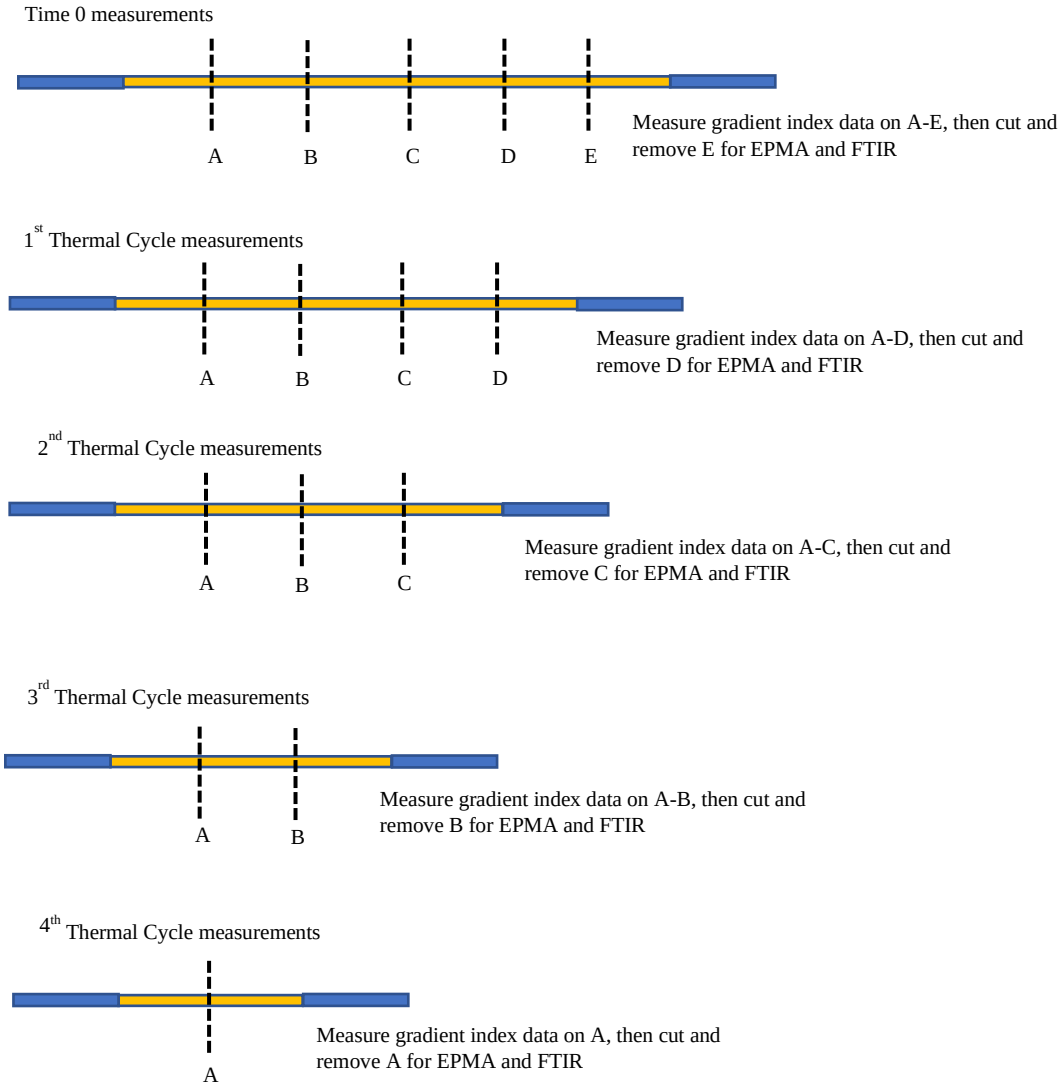

Figure 35: A sample plan to repeat this experiment with EPMA and FTIR to track where the alkali and water meet.

E. Total Concentration

The total concentration theoretically should remain constant since there is a fixed amount of potassium ions in the silica network. The concentration was calculated by converting the gradient index data to wt% K_2O then using Equation *14*, which divides the area under the curve of the gradient profile by the total cross-sectional area of the cane.

Equation 14 $$ppm\ K_2O = \frac{10{,}000\pi\left(\frac{1}{2}\right)\sum_{-ExtentK}^{+ExtentK} wt\%(x)\left|r_{i+1}^2 - r_i^2\right|}{Area}$$

Figure 36 shows the calculated concentration for each thermal cycle. The values are relatively consistent until the fourth thermal cycle, when the concentration significantly increases. This increase is not possible due to conservation of mass and the fixed amount of potassium in the glass.

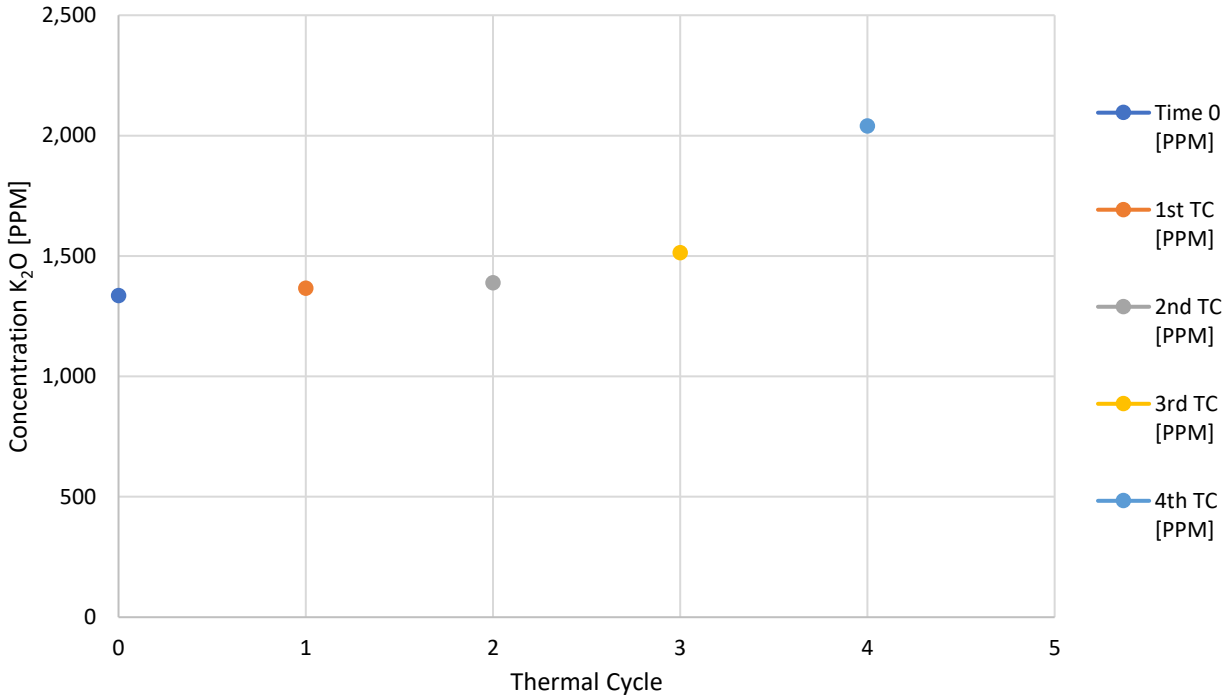

Figure 36: The total concentration of potassium for each cycle shows a slight increase with each thermal cycle.

An important thing to consider for the concentration summation of Equation 14 is the drop in peak potassium shown by the gradient curves in Figure 26 and Figure 27. The peak potassium significantly dropped from Time Zero to the first thermal cycle, decreasing by 0.2mol% K_2O. But after that, the peak height remained constant, only changing a total of 0.05mol% K_2O from the first to the fourth cycle.

The initial drop in index peak may indicate an error in the assumption that only the potassium in the core affects the gradient index. There could be another factor causing the increase in index in

the initial sample. The SEM and EDX data support the hypothesis that the increase in gradient index is from potassium, but the EDX and SEM cannot measure stress in the cane. If the glass was stressed during fabrication, that stress would anneal out during the first thermal cycle, causing the initial drop in the peak index.

The source of stress is thought to be chemical differences through the glass, not other index modifiers such as thermal stress. The cooling rate of the cane can be calculated using the thermal cycling rates in Figure 11. At 2mm/min, the sample cooled at about 44°C/min. The burner traverse during cane fabrication was 10.5mm/min, and while no thermal profile data was collected at this rate, the profile should be the same since the same burner and flow rates were used. Therefore, the cooling rate would have been about 228°C/min.

However, Figure 36 contradicts the assumption of additional thermal stress altering the gradient index profile because of the cooling rate. Figure 36 shows consistent concentration data from Time Zero through the third thermal cycle, but then a significant increase in the concentration after the fourth thermal cycle.

The cooling rate's effect on the gradient index profile could be tested by changing the burner traverse speed for a thermal cycle. If the gradient index peak dropped after the first thermal cycle at 2mm/min, would the peak rise back up if the next thermal cycle was run at 10.5mm/min? This experiment would not be ideal when determining diffusion coefficients, but it would be an interesting tangent.

The difference in gradient index peaks does not appear to affect the total diffusion rate but should be considered in further experimentation.

IV. CONCLUSION

This work concludes that the average diffusion coefficient for a peak of ~1.2mol% potassium oxide concentration to diffuse in silica glass when exposed to a temperature of 1856°C is $D = (1.23 \pm 0.54) \times 10^{-6}$ cm^2/second. The diffusion rate of potassium may have been influence by water in this case, which diffused from the cane's surface into the glass due to long exposure to the hydro-oxygen burner.

The diffusion coefficient agrees with published literature. Rothman's [2] data is at lower temperatures, but it aligns with the Arrhenius model of data from this experiment. The use of gradient index profiles is a viable method for obtaining non-destructive radial measurements of alkali diffusion in a glass cane.

Further study could be done on the thermal stress of a cane with no alkali. Additionally, different alkalis could be studied to expand on the literature about diffusion coefficients at high temperatures.

V. REFERENCES

[1]. Tamura, Y.; Haruna, T.; Saito, Y.; Kawaguchi, Y.; Hirano, M. OPTICAL FIBER HAVING AN ALKALI METAL DOPED SILICA GLASS CORE, July 6, 2016.

[2]. Rothman, S. J.; Marcuso, T. L. M.; Nowicki, L. J.; Baldo, P. M.; McCormick, A. W. Diffusion of Alkali Ions in Vitreous Silica. *Journal of the American Ceramic Society* 1982, *65* (11), 578–582.

[3]. Frischat, G. H. *Ionic diffusion in Oxide Glasses*; Trans Tech Publications: Clausthal, Ger., 1975.

[4]. Smith, C. M. Silica, Vitreous. *Kirk-Othmer Encyclopedia of Chemical Technology* 2006.

[5]. Lewis, J. A. The Collapse of a Viscous Tube. *Journal of Fluid Mechanics* 1977, *81* (01), 129.

[6]. Klupsch, T.; Pan, Z. Collapsing of Glass Tubes: Analytic Approaches in a Hydrodynamic Problem with Free Boundaries. *Journal of Engineering Mathematics* 2017, *106* (1), 143–168.

[7]. Kirchhof, J. Reactor Problems in Modified Chemical Vapour Deposition (i). the Collapse of Quartz Glass Tubes. *Crystal Research and Technology* 1985, *20* (5), 705–712.

[8]. Kirchhof, J.; Funke, A. Reactor Problems in Modified Chemical Vapour Deposition (II). the Mean Viscosity of Quartz Glass Reactor Tubes. *Crystal Research and Technology* 1986, *21* (6), 763–770.

[9]. Kirchhof, J.; Unger, S.; Dellith, J.; Scheffel, A.; Teichmann, C. Diffusion Coefficients of Boron in Vitreous Silica at High Temperatures. *Optical Materials Express* 2012, *2* (5), 534.

[10]. Kirchhof, J.; Unger, S.; Klein, K.-F.; Knappe, B. Diffusion Behaviour of Fluorine in Silica Glass. *Journal of Non-Crystalline Solids* 1995, *181* (3), 266–273.

[11]. Kirchhof, J.; Kleinert, P.; Radloff, W.; Below, E. Diffusion Processes in Lightguide Materials. the Diffusion of Oh in Silica Glass at High Temperatures. *Physica Status Solidi (a)* 1987, *101* (2), 391–401.

[12]. Kirchhof, J.; Unger, S.; Dellith, J. Diffusion of Phosphorus Doped Silica for Active Optical Fibers. *Journal of Non-Crystalline Solids* 2004, *345-346*, 234–238.

[13]. Photon kinetics, optical fiber preform analyzers from photon kinetics. http://www.pkinetics.com/products/productdetail.aspx?model=p104 (accessed Apr 2, 2022).

[14]. Watkins, L. S. Laser Beam Refraction Traversely through a Graded-Index Preform to Determine Refractive Index Ratio and Gradient Profile. *Applied Optics* 1979, *18* (13), 2214.

[15]. Heraeus. Quartz Glass Tubes. Retrieved November 26, 2020, from https://www.heraeus.com/en/hca/products_hca/tubes_1/tubes_semi_1/tubes_semiconductor_application_hca.html

[16]. Lines, M. E. Can the Minimum Attenuation of Fused Silica Be Significantly Reduced by Small Compositional Variations? I. Alkali Metal Dopants. *Journal of Non-Crystalline Solids* 1994, *171* (3), 209–218.

[17]. Schroeder, J. Brillouin Scattering and Pockels Coefficients in Silicate Glasses. *Journal of Non-Crystalline Solids* 1980, *40* (1-3), 549–566.

[18]. Bansal, N. P.; Doremus, R. H. In *Handbook of glass properties*; Elsevier: New Delhi, 2006; pp 539–606.

[19]. Anderson, O. L.; Stuart, D. A. Calculation of Activation Energy of Ionic Conductivity in Silica Glasses by Classical Methods. *Journal of the American Ceramic Society* 1954, *37* (12), 573–580.

[20]. Nascimento, M. L.; Dantas, N. O. Anderson-Stuart Model of Ionic Conductors in Na2O-SiO2 Glasses. *Ciencia and Engenharia/ Science and Engineering Journal* 2003. 12. 7.

[21]. Nascimento, M. L.; Watanabe, S. Test of the Anderson–Stuart Model and Correlation between Free Volume and the ‘Universal’ Conductivity in Potassium Silicate Glasses. *Materials Chemistry and Physics* 2007, *105* (2-3), 308–314.

[22]. Nascimento, M. L.; Nascimento, E. do; Watanabe, S. Test of Anderson-Stuart Model and the "Universal" Conductivity in Rubidium and Cesium Silicate Glasses. *Brazilian Journal of Physics* 2005, *35* (3a), 626–631.

[23]. Nascimento, M. L. Test of the Anderson–Stuart Model and Correlation between Free Volume and the ‘Universal’ Conductivity in Sodium Silicate Glasses. *Journal of Materials Science* 2007, *42* (11), 3841–3850.

[24]. McElfresh, D. K.; Howitt, D. G. Activation Enthalpy for Diffusion in Glass. *Journal of the American Ceramic Society* 1986, *69* (10).

[25]. Charles, R. J. Metastable Liquid Immiscibility in Alkali Metal Oxide-Silica Systems. *Journal of the American Ceramic Society* 1966, *49* (2), 55–62.

[26]. Mehrer, H. In *Diffusion in solids: Fundamentals, methods, materials, diffusion-controlled processes*; 155; Springer: Berlin, 2007; pp 27–67.

[27]. Varshneya, A. K.; Mauro, J. C. In *Fundamentals of Inorganic Glasses*; Elsevier: Amsterdam, 2019; pp 383–424.

[28]. Bockris, J. O. M.; Mackenzie, J. D.; Kitchener, J. A. Viscous Flow in Silica and Binary Liquid Silicates. *Transactions of the Faraday Society* 1955, *51*, 1734.

[29]. Mazurin, O. V.; Strel'cina, M. V.; Svajko-Svajkovskaja, T. P. In *Handbook of glass data*; 1983; pp 432–432.

[30]. Doremus, R. H. Viscosity of Silica. *Journal of Applied Physics* 2002, *92* (12), 7619–7629.

[31]. Avramov, I. Relationship between Diffusion, Self-Diffusion and Viscosity. *Journal of Non-Crystalline Solids* 2009, *355* (10-12), 745–747.

[32]. Berezhnoi, G. V.; Boiko, G. G. Defects and Oxygen Diffusion in Metasilicate Melts: Molecular Dynamics Simulation. *Glass Physics and Chemistry* 2005, *31* (2), 145–154.

[33]. Scholze, V. H.; Mulfinger, H. Der Einbau des Wassers in Gläsern, V. Die Diffusion des Wassers in Gläsern bei hohen Temperaturen, *Glastechnische berichte* 1959, 32, 381-386